frontiers in Environmental Science

ORIGINAL RESEARCH
published: 11 January 2022
doi: 10.3389/fenvs.2021.800517

Geo-Temporal Signatures of Physicochemical and Heavy Metals Pollution in Groundwater of Khulais Region—Makkah Province, Saudi Arabia

Mohd Yawar Ali Khan[1]*, *Mohamed El Kashouty*[1], *Waleed Gusti*[1,2], *Amit Kumar*[3], *Ali Mohammad Subyani*[1] and *Ahmed Alshehri*[4]

[1]Department of Hydrogeology, Faculty of Earth Sciences, King Abdulaziz University, Jeddah, Saudi Arabia, [2]Department of Environmental Sciences, Faculty of Meteorology, Environment and Arid Land Agriculture, King Abdulaziz University, Jeddah, Saudi Arabia, [3]School of Hydrology and Water Resources, Nanjing University of Information Science and Technology, Nanjing, China, [4]Department of Engineering and Environmental Geology, Faculty of Earth Sciences, King Abdulaziz University, Jeddah, Saudi Arabia

OPEN ACCESS

Edited by:
Khalid Muzamil Gani, National Institute of Technology, India

Reviewed by:
Saurabh Mishra, Hohai University, China
Rudra Mohan Pradhan, Indian Institute of Technology Bombay, India

***Correspondence:**
Mohd Yawar Ali Khan
yawar.gr44@gmail.com

Specialty section:
This article was submitted to Water and Wastewater Management, a section of the journal Frontiers in Environmental Science

Received: *23 October 2021*
Accepted: *14 December 2021*
Published: *11 January 2022*

Citation:
Khan MYA, El Kashouty M, Gusti W, Kumar A, Subyani AM and Alshehri A (2022) Geo-Temporal Signatures of Physicochemical and Heavy Metals Pollution in Groundwater of Khulais Region—Makkah Province, Saudi Arabia. Front. Environ. Sci. 9:800517. doi: 10.3389/fenvs.2021.800517

Seawater has intruded into many of Saudi Arabia's Red Sea coastal aquifers, with varying degrees of extension depending on location, hydrogeology, and population density. This study aimed to evaluate and comprehend the processes that influence the hydrogeochemical characteristics of the coastal aquifer in Saudi Arabia's Khulais region. Groundwater samples were taken from nineteen locations during the winter and summer of 2021, and data from major ions and trace elements were examined and interpreted using ArcGIS software. The total dissolved solids (TDS) concentrations ranged between 480 and 15,236 mg/L and 887–18,620 mg/L in winter and summer, respectively. Groundwater TDS concentration was observed to be influenced by groundwater flow, lithogenic, anthropogenic, and seawater intrusion in this study (2021) when compared to 2016. The concentration of nitrate (NO_3^-) and strontium (Sr) in most samples exceeds the drinking guidelines. The occurrence of high concentrations of bromide (Br), Fluoride (F), Iron (Fe) (winter and summer) and Aluminum (Al), Boron (B), Chromium (Cr), Nickel (Ni), lead (Pb), cadmium (Cd), cobalt (Co), copper (Cu) and manganese (Mn) (winter) was also exhibited and observed up to more than drinking and irrigation limits. The central part of the study area was affected by seawater intrusion. The hydraulic conductivity of the topsoil was measured, and it ranged from 0.24 to 29.3 m/day. Based on electrical conductivity (EC) and sodium absorption ratio, most aquifer samples were unsuitable for irrigation (SAR).

Keywords: major ions, toxic metals, aquifer, seawater intrusion, Saudi Arabia

1 INTRODUCTION

Water scarcity affects almost two billion people, or 35% of the world's population, due to rapid population growth and agricultural area expansion and degradation (Alcamo et al., 2000; Wada et al., 2010; Kumar et al., 2021a; Kumar et al., 2021b; Mishra et al., 2021). Coastal aquifers are among the most critical water sources in coastal areas, providing water to over a billion people and supporting agricultural and industrial activities (Ferguson and Gleeson, 2012). Overexploitation of groundwater

is common as a result of population growth to fulfill the tremendous demand for water for drinking water and irrigation, resulting in deterioration of groundwater quality, decreased groundwater levels, and seawater intrusion into coastal aquifers. Sources of aquifer degradation include lithogenic, anthropogenic, and seawater intrusion. Anthropogenic pollution comes from industrial effluents, fertilizers, pesticides, domestic wastewater and landfills (Khan et al., 2016; Pradhan and Biswal, 2018; Li et al., 2019; Kumar et al., 2021c; Khan and Wen, 2021). Hydrogeochemical and isotopic studies have been conducted to assess groundwater quality and better understand hydrological and salinization processes in various coastal aquifer systems around the world (Rosenthal, 1987; Vengosh and Rosenthal, 1994; Allen and Suchy, 2001; Lee and Song, 2007; De Montety et al., 2008; Skrzypek et al., 2013; Khan et al., 2017; Behera et al., 2019; Khan et al., 2020; Pradhan et al., 2021). Saltwater pumping, inter-aquifer mixing, palaeo-saline water, anthropogenic contamination, rock–groundwater interaction, and other factors contribute to groundwater salinization in coastal areas (Han et al., 2014; Larsen et al., 2017). The spread of microorganisms to humans occurs when wastewater contaminates groundwater (WHO, 1993; WHO, 1994; WHO, 2004). The amount of coastal groundwater discharged for various purposes has increased, putting it at risk of misuse and contamination. As a result, there is a severe deterioration in groundwater quality and a high concentration of TDS in the groundwater.

Saudi Arabia's total runoff (2,200 million m^3/year) contributed to shallow groundwater inflows (Food and Agriculture Organization of Uthe nited Nations, 2009). Water consumption has recently fluctuated dramatically due to population increase and the need for survival. Water use has climbed from 2,352 million m^3/year in 1980 to over 20,000 million m^3/year in 2004 (irrigation needs > 88 percent) (Jabr et al., 2017). Groundwater accounts for 75–85 percent of the country's water resources (Abderrahman, 2006). Saudi Arabia's aquifers have been replenished at a 1.28 billion m^3/year rate, whereas 394 million m^3/year has been drained (Ministry of Planning). The shallow aquifer is renewable, with a capacity of 950 billion m^3, whereas the (non-renewable) deeper aquifer has a capacity of 500,000 billion m^3 (Al-Ibrahim, 1991).

According to the Ministry of Environment, Water and Agriculture, drinking water consumption in Saudi Arabia has increased yearly (**Supplementary Figure S1A**). Desalinated water represented 63% (2.14 billion m^3) of the water distributed per year, while groundwater represented 37% or 1.26 billion m^3. According to the report, the total water demand for different uses in 2017 and 2018 (**Supplementary Figure S1B**) was 23.350 and 25.99 billion m^3 (rises 8%), respectively (https://www.argaam.com/en/article/articledetail/id/1312492).

Khulais is a governorate in Saudi Arabia's southernmost province, Makkah. It was historically considered a prominent region since it served as a rest stop for pilgrims travelling between Makkah Al Mukaramah and Madinah Al Munawarah. It is around 30 km from the Red Sea's coast (**Figure 1**). Surface waterways are scarce, and groundwater is the only source of water. Natural and anthropogenic influences are both harmful to the shallow aquifer. The hydrological input is lower than the production. As a result, its ecosystem is unbalanced, resulting in significant groundwater pollution due to seawater intrusion and agricultural effects. The most severe and visible issue is the rapid depletion of groundwater resources, caused by declining groundwater levels, pollution, or a combination of the two. Groundwater is becoming too expensive to use, resulting in low agricultural outcomes. Therefore, the main objectives of the present study are to define the aquifer's physical and chemical properties, identify pollution sources, calculate the rate of seawater intrusion, and assess the aquifer's functions. Once seawater intrusion has been identified, hydrogeologists monitor, plan, and conserve the aquifer. Otherwise, there will be a water shortage, posing a threat to groundwater development.

2 MATERIALS AND METHODS

2.1 Study Area

The Khulais Plain is located roughly 110 km north-east of Jeddah, Saudi Arabia, between latitudes 22°00′–22° 15′ N and longitudes 39°05′–39°30′ E (**Figure 1**). Wadi Abu Hulaifa, Wadi Murawani, and Wadi Ghiran are the three main Wadis that drain into the plain. Wadi Khulais was once used for agriculture, and its groundwater served as a source of drinking water. The region has a dry climate. Summer temperatures range from 30 to 34°C, while winter temperatures range from 20 to 24°C. The average annual rainfall in the west (flat parts) is 60 mm/y, whereas it rises to more than 170 mm/y in the east (mountainous areas) (Gabr et al., 2017). Because of the uneven distribution and torrential nature of the rainfall, groundwater recharge is very transitory.

2.2 Geology

A Precambrian and Cambrian crystalline basement complex is overlain unconformably by a Cretaceous-Tertiary sedimentary succession in the area (**Supplementary Figure S2**). Basalt flows from the Tertiary and Quaternary periods have covered both rock units in places. The youngest unit of the sequence is the Quaternary-recent deposits, including the sediments deposited by the Wadis. Elevated basement outcrops provide a structural boundary on the plain's eastern and western margins, generating a downthrown graben structure (Bazuhair et al., 1992). The area's fault system runs parallel to the Red Sea graben and can be seen in the basement rocks. Basement rocks are also affected by dyke swarms and sills.

2.3 Hydrogeology

The transmissivity of the aquifer ranged from 90 to 5,800 m2/day, with hydraulic conductivity ranging from 7 to 1,035 m/day and porosity of 25–35% (Hussein et al., 1993; Hussein et al., 1993). The unconfined nature of Tertiary and Quaternary sediments represent the aquifer system (**Supplementary Figure S3A–C**). The Quaternary aquifer is an alluvial fan composed of conglomerates overlaid by sandstones and siltstones, characterized by cross-bedded and laminated (Sonbul et al., 2017). The alluvial fan of Wadi Khulais contains a high Quaternary aquifer thickness (Gabr et al., 2017) and recharge

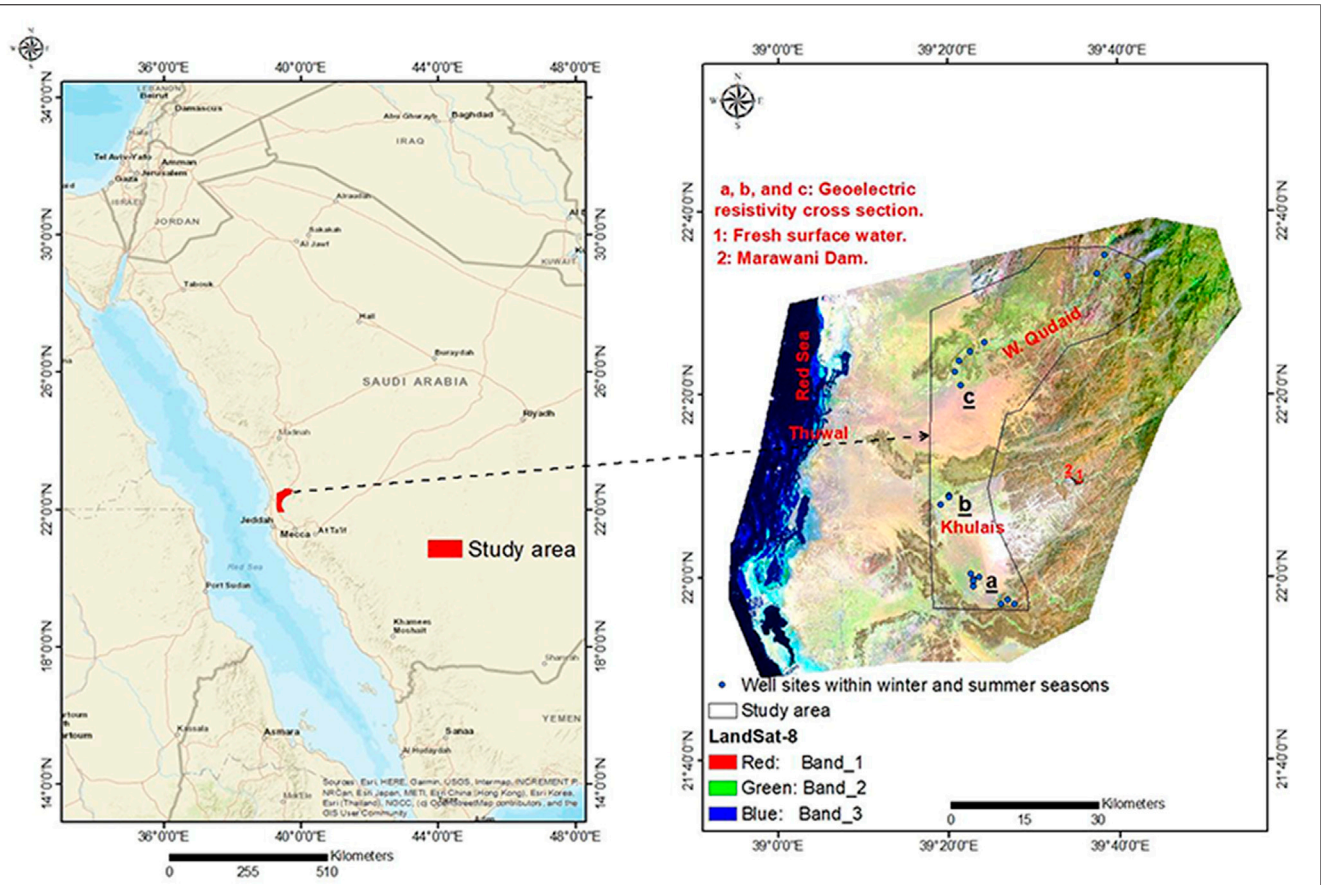

FIGURE 1 | A Landsat-8 false color composite image (bands 7, 5, 3 in RGB).

by precipitation. It is attributed to geomedia dissolution (dolomite in the dolomitic tuff, basic tuffs, and ferromagnesian minerals) and seawater intrusion that the Tertiary aquifer (structurally regulated) is saturated with saline water. The Quaternary-Tertiary aquifers are hydrogeologically linked and considered as a single unit.

2.4 Samples Collection and Analysis

Nineteen sampling locations that were selectively chosen and monitored at the studied region are shown in **Figure 1**. Groundwater samples were taken from each sampling site's borehole in the summer and winter of 2021, protected, and transferred to the laboratory using standard precautions (APHA, 1998). The containers were first treated with nitric acid (HNO_3) and then rinsed with the groundwater twice at the sampling locations to avoid any contamination. To reduce the margin of error, the filtering process was carried out within 2 days of collecting the samples, stored in a refrigerator at 4°C to avoid the growth of organic matter. All samples were filtered using a 0.45 µm cellulose nitrate membrane. Digital meters (HACH Instruments) were used to measure each water sample's pH and electrical conductivity (EC). TDS and temperature were measured by using an automatic TDS meter (HACH Instruments) and a Mercury thermometer (HACH Instruments), respectively. Ion chromatographer (IC) (Metrohm 850 Professional IC) was used to determine the concentration of cations and anions. The IC was calibrated by using a standard solution of cations and anion eluents. The IC detection limit of various cations and anions was 0.1 mg/L. The concentrations of heavy metals were measured by an Inductive Coupled Plasma Optical Emission Spectrometer (ICP-OES) (Agilent ICP 720ES) according to the procedure recommended by Environmental Protection Agency (EPA, Method 3005A). These analyses (heavy metals and ions) were performed in the Center of Excellence in Desalination Technology at King Abdulaziz University, Jeddah, Saudi Arabia.

Sixteen soil samples were also collected from the top alluvium shallow aquifer (<1.5 m depth) using a hand auger to assess the hydraulic conductivity (K) and grain size analysis. The granulometric investigation was done for sixteen dry soil samples using sieves 4, 2, 1 mm, 710, 500, 300, 250, 125, 63, and <63 µm. The test applies the ASTM (1980), the sieving investigation, by GradiStat excel file, determine the granulometric parameters shown in **Table S5**. The K of the soil samples were estimated using the Hazen equation (Hazen, 2013)

$$\mathbf{K(m/d) = C(constant) * (D10)^2} \quad (1)$$

Two images (Path/row was 170/45 and 170/44) of Shuttle Radar Topography Mission–Digital Elevation Model (SRTM-DEM) 30 m resolution was collected from United States

TABLE 1 | Mean values of groundwater quality parameters of Khulais region.

Parameters	Winter, 2021	Summer, 2021
Physicochemical		
pH	7.672 ± 0.255	7.141 ± 0.32
TDS	4,145.525 ± 3,403.51	5,343.075 ± 4,484.655
EC	7,773.403 ± 6,270.478	10,309.557 ± 8,870.472
Cl^-	1,585.541 ± 1,620.117	2,278.828 ± 2,554.127
NO_3^-	65.952 ± 82.962	90.552 ± 96.739
SO_4^-	930.026 ± 531.925	971.017 ± 581.469
HCO_{3-}	190.067 ± 46.429	269.33 ± 80.922
Na	696.805 ± 696.389	889.632 ± 795.745
K	15.423 ± 18.703	17.257 ± 24.415
Mg	172.156 ± 173.442	244.154 ± 215.975
Ca	481.396 ± 467.309	571.701 ± 528.393
Heavy Metals		
Al	0.904 ± 0.548	—
B	0.927 ± 0.561	—
Ba	0.146 ± 0.049	—
Co	0.047 ± 0.038	—
Cr	0.103 ± 0.065	—
Cu	0.521 ± 0.302	—
Fe	0.171 ± 0.094	0.019 ± 0.035
Mn	0.264 ± 0.549	—
Ni	0.075 ± 0.059	—
Pb	0.399 ± 0.245	—
Zn	0.035 ± 0.031	—
F	1.547 ± 0.353	1.427 ± 0.564
Br	6.451 ± 6.639	9.344 ± 9.968
Se	—	0.017 ± 0.014
Sr	—	5.688 ± 5.801

Geological Survey (USGS) website (http://earthexplorer.usgs.gov/). In addition, two ETM+ (Enhanced Thematic Mapper Plus) images (LANDSAT_PRODUCT_ID = ″LC08_L1TP_170045_20190303_20190303_01 and LANDSAT_PRODUCT_ID = ″LC08_L1TP_170044_20190303_20190303_01) of Landsat-8 with 30 m resolution was downloaded from the USGS website. The DEM and Landsat images were mosaic by using ArcGIS 10.3 software. These mosaicked images were used to prepare a base map for the respective region. The lineaments delineation steps respectively are extraction by Envi v 5.1; automatic extraction lineaments [using principal component image (PCI)]; handling extraction lineaments (ArcGIS 10.3); and trend analysis (RockWork v 16). SRTM-DEM image was used to prepare thematic maps of elevation and drainage basins.

3 RESULTS AND DISCUSSION

Groundwater salinization, salt-water encrustation, lithogenic, and anthropogenic pollution are the principal threats to the aquifer supply in the arid Khulais region. As a result, the source and mechanisms of water salinization must be revealed to implement an effective strategy for restoring and managing the aquifer's quality. The evolution of groundwater has been proven in the following sections using hydrogeochemical processes in the aquifer.

3.1 Hydrogeochemsitry

The hydrogeochemistry of groundwater has been reviewed in this section based on TDS, cations, anions, and hazardous metals concentrations that were distributed and analyzed throughout the investigation region. The aquifer has been classed as suitable or unsuitable for consumption and irrigation based on water concentration levels.

3.1.1 TDS and EC

Table 1 shows the mean values of physicochemical parameters and heavy metal concentrations in the groundwater of the studied area. **Figure 2A** shows that TDS concentrations rise from 1,000 ppm in the northeast to 15,000 ppm in the central-western region in winter due to seawater intrusion through the Wadi Khulais' open Quaternary deposits, are not hindered by hard rocks (**Supplementary Figure S2**). The aquifer's shallow depths and the thickness of alluvial deposits (more than 200 m) allow for a high rate of seawater penetration (**Supplementary Figure S3**). Tihamat al Hijaz is a thick Tertiary clastic succession (mainly sandstone) overlain by Tertiary basalt and Quaternary deposits in the western coastal area (Gabr et al., 2017). It facilitates the flow of seawater into the aquifer. Seawater intrusion is limited by Hammah basalt in the northeastern and central-southern parts (lowest TDS content) (Rahat group). The maximum rainfall (>1,500 mm/y) was recorded in the northeast [488–1011 m above mean sea level (a.m.s.l)], which can infiltrate and recharge the aquifer system (**Figure 2C**). The TDS concentration increases with groundwater flow (northeast to central-western part) due to the breakdown of geomedia dissolution (such as dolomitic tuff, basic tuffs, and ferro-magnesian minerals) (**Supplementary Figure S2**).

It is clear from **Figures 2A**,**B**, **3A** that hydrogeology (groundwater flow) and hydro-geochemistry are related (TDS concentration). The TDS concentration increases from 3,000 ppm (discharge zone) to 5,000 ppm (recharge zone) in the southeast (**Figure 2A**), indicating that there is no relationship between groundwater flow and TDS concentration. It could be due to a decrease in seawater intrusion rate due to changes in Quaternary deposit thickness and facies.

The percentage of gravel in the top soil layer increases as TDS concentration decreases (**Section 3.5**), indicating that rainwater penetration into the aquifer system is considerable. **Figure 3B** depicts an increase in lineaments density in the northeastern region, where TDS concentrations are reduced due to increased rainfall penetration through these densely packed lineaments. The overall length of the lineaments is 1,262.5 km (**Supplementary Table S1**). From the 9,626.8 km of the basin boundary, the study area consists of six orders with a total length of 2,428.2 km (**Figure 3C**, **Supplementary Table S2**). The seawater intrusion rate was higher in the upper central part (lower elevation) than in the lower (higher elevation) (**Figure 2C**). When compared to lower elevations, the rate of seawater intrusion was lower at higher elevations.

TDS concentrations in the summer ranged from < 1,000 to 185,000 ppm, following the winter trend but with high seawater intrusion and across a larger area (**Figure 2B**). During the summer of 2016, TDS concentrations ranged from 550 to 12,850 ppm (Saleem and Algamal, 2016), and the distribution pattern matches the current study. TDS concentration map in summer was eliminated from TDS levels in winter and 2016

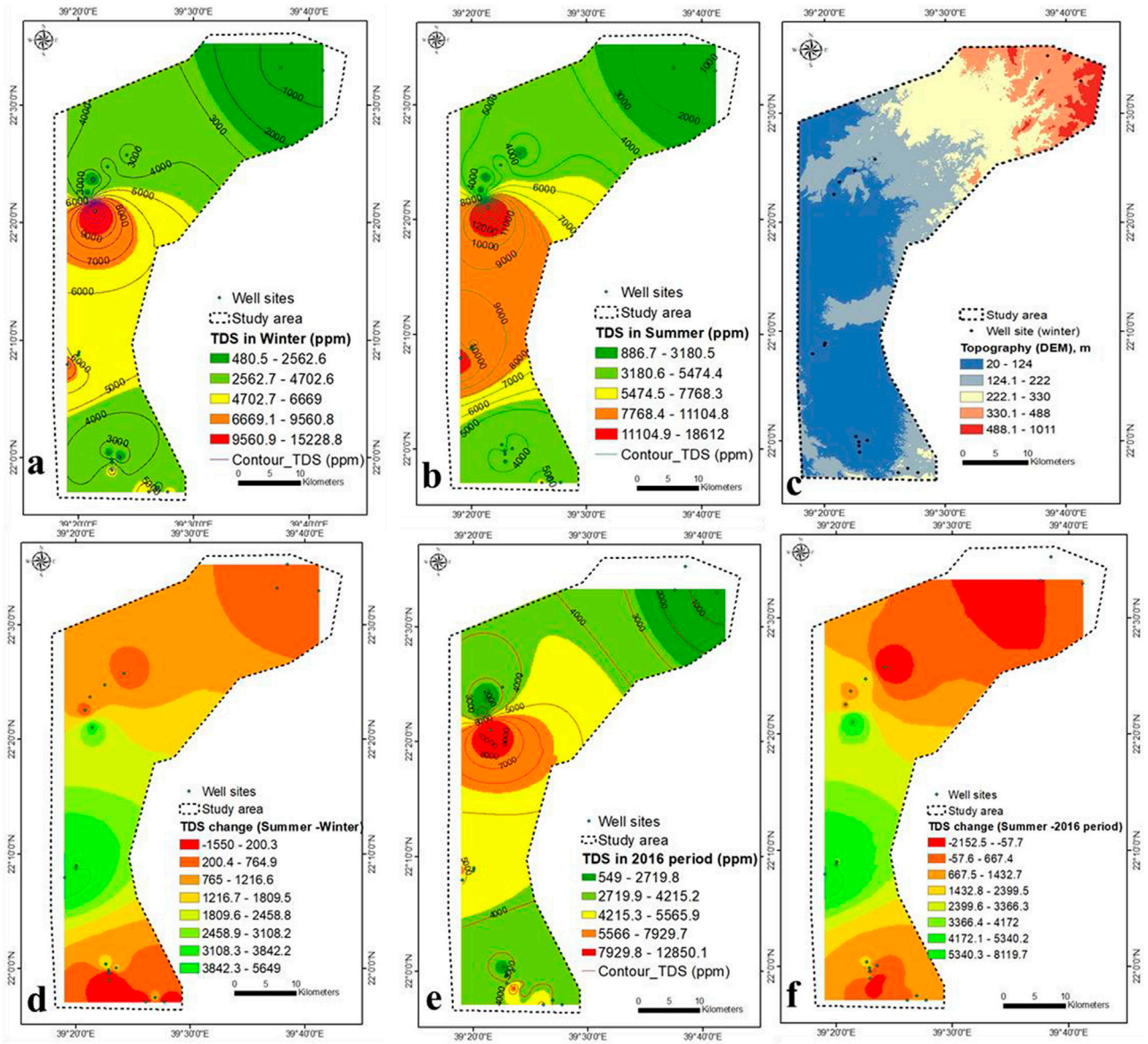

FIGURE 2 | (A,B) TDS concentration during winter and summer 2021 (this study), **(C)** topography, **(D)** TDS variation in winter-summer, **(E)** TDS concentration during 2016, and **(F)** TDS variation in summer of 2021 (this study) and 2016 (Saleem and Algamal, 2016).

period by Map Algebra (GISARC Map). In most regions, TDS concentrations rise in the summer compared to the winter (**Figure 2D**). It is related to extremely light rainfall throughout the summer, while rainfall reaches 4–9 mm/d during the winter (**Supplementary Figure S4**). The maximum TDS increase was found in the central part by 2,459–5,649 ppm, attributed to high pumping rate, scarce rainfall (**Supplementary Figure S4A**), low aquifer recharge, high evaporation, and seawater intrusion.

Compared to the TDS concentration of 2016 (Saleem and Algamal, 2016) (**Figure 2E**), the maximum variation was found in the central part, ranging from 2,400 ppm (2016) to 8,120 ppm (present study) ppm (**Figure 2F**). It may be attributed to the low recharge, high pumping rate, high rate of seawater intrusion, high evaporation, and unmanaged wells. The change in precipitation from more than 100 mm/y (2016) to less than 50 mm/y (2021) caused increases in TDS concentration in 2021. The values of EC in winter and summer ranged from 874 to 27,689 and 1,673–36,494 μS/cm, respectively (**Figures 4A,B**). The changes in EC values are similar to that of TDS concentration (**Figure 4C**).

3.1.2 Cations and Anions

The concentrations of Na, K, Ca, Mg and Cl follow the same trend as that of TDS (**Figures 5**, **6**). During the winter and summer, the concentration of SO_4^- was similar to that of TDS, with the exception of the south-eastern region, where it increased due to rock-water interaction (**Figures 6E,F**).

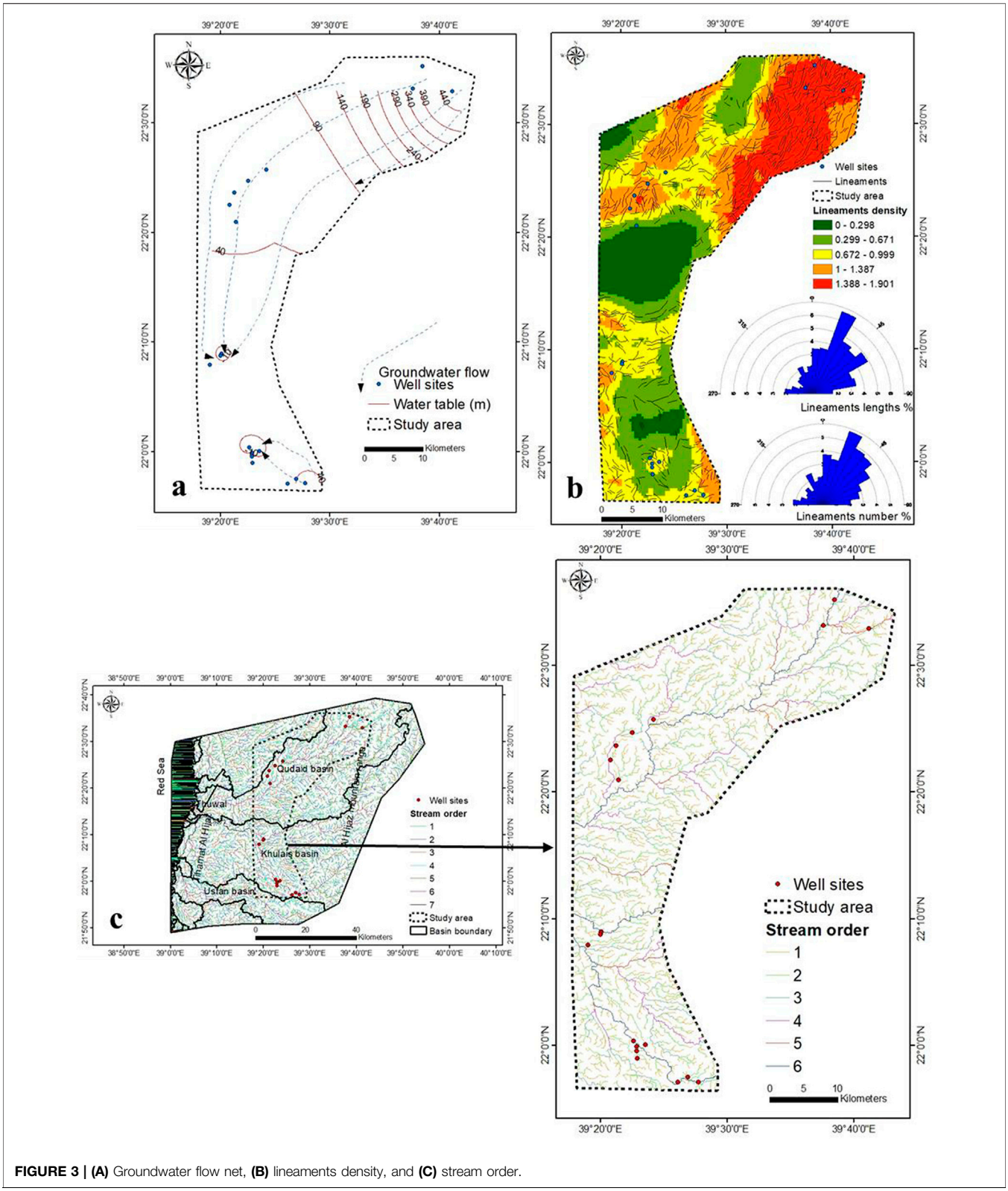

FIGURE 3 | (A) Groundwater flow net, **(B)** lineaments density, and **(C)** stream order.

The southeastern part is characterized by presence of hornblende tonalite (Shiwan compex), Amudan Formation (Samran group), Hammaha basalt and Bathan Formation (Rahat group). The dissolution of these sediments contributed partially to the concentration of SO_4^- in the aquifer in southeastern part. However, SO_4^- concentration in

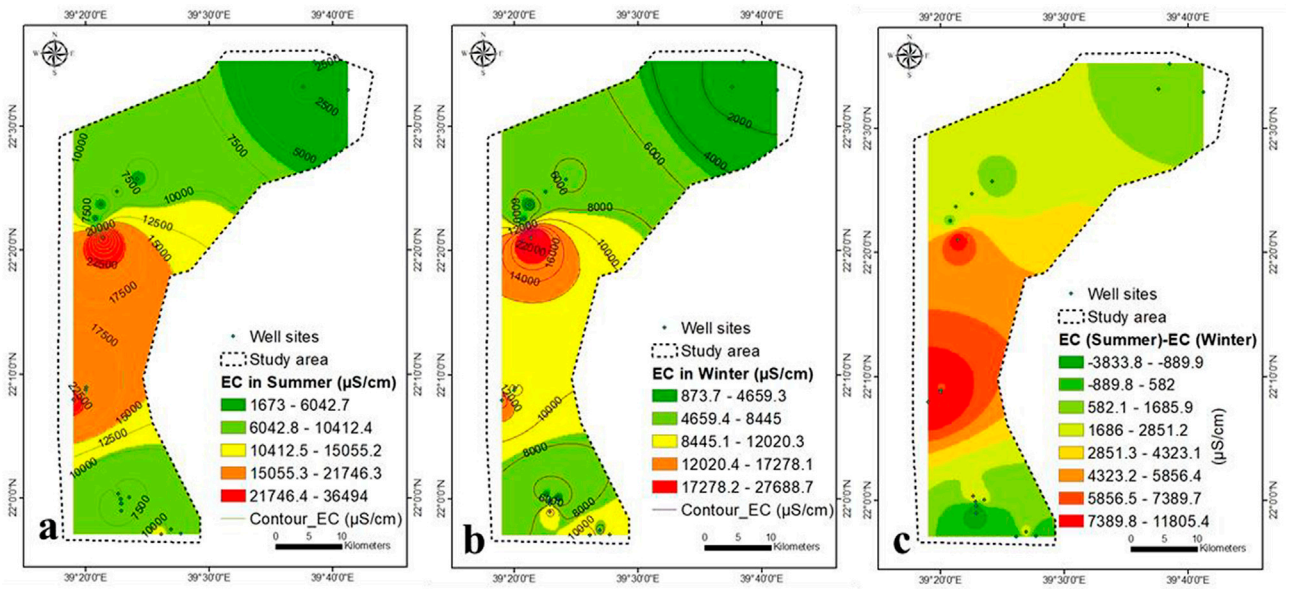

FIGURE 4 | EC concentration in **(A)** winter, **(B)** summer, and **(C)** variation is winter and summer.

groundwater was also contributed by seawater intrusion. The weakest correlation between TDS and ions was that of TDS- SO_4^- (r = 0.84 in winter and 0.76 in summer) and might be due seawater intrusion and rock water interaction. The HCO_3^- concentration increases in winter due to the upper central and south-eastern parts (**Figure 7A**), while it increases in summer due to the main north-eastern part and the lower central part (**Figure 7B**).

3.1.3 NO_3^- Concentration

The NO_3^- content in groundwater ranges from 1.5 to 338 mg/L during winter and summer, with values above permissible limits in most regions (**Figures 7C,D**). It might be attributed to agrochemicals used for agricultural practices, which enhance the nitrification process in the aquifer systems. The heterogeneous aquifer system (dramatic change in the TDS concentration) exhibits a great diversity of NO_3^- content. The massive agricultural industry, land use and organic fertilizer applications more often contributed to the higher concentration of NO_3^- in groundwater (Zarhloule et al., 2009; Fekkoul et al., 2013). Depending on the difference in water depth (20–120 m), groundwater refers to two different sources of pollution, point and non-point (agricultural, septic tanks, animal waste dump and cesspools). It is evident from **Table 2** that there is no correlation between the concentration of NO_3^- and TDS (0.08), suggesting that contamination by NO_3^- is mainly attributed to agricultural activities.

The central part has an average concentration of NO_3^- and a very high concentration of TDS, indicating the effect of agricultural wastewater and seawater intrusion. Most groundwater samples during winter and summer exceed the maximum level of NO_3^- pollutants for drinking consumption (45 mg/L, WHO, 2017). The NO_3^- concentration in 2016 was <50–385 mg/L (Saleem and Algamal, 2016), higher than that of the current values (**Figure 7G**). In summer, most samples show a higher concentration of NO_3^- compared to winter (**Figure 7E**), which may be due to the higher fertilizer application in summer than in winter. The increase in NO_3^- concentration was highest (30–142 mg/L) in the lower central to southeastern parts (**Figure 7E**).

The health risk assessment of a drinking water source can establish a link between pollution and human health (Wang et al., 2015). Two pathways for trace elements to transfer into the human body from groundwater are ingestion (drinking) and dermal (showering). Recent researches show that the dangers posed by ingesting contaminated groundwater are two to three orders of magnitude greater than those posed by the dermal pathway (Li et al., 2015c; Wu and Sun, 2016; Yin et al., 2021).

The concentration of NO_3^- in the aquifer is considered a severe pollution source (Chen et al., 2016; Adimalla and Li, 2018). NO_3^- pollution in the aquifer of western Iran is caused by agricultural activity (Jalali, 2011), while in northwest China, it is attributed to the rate of fertilizer, intensive irrigation and high permeability (Chen et al., 2016). High levels of NO_3^- in the aquifer are harmful to humans with continued ingestion, especially methemoglobinemia or blue baby syndrome, esophageal and stomach cancer, and thyroid hypertrophy (Adimalla and Qian, 2019).

3.1.4 Toxic Metals

The Br concentration was high throughout the study area and varied between 0.65–15.5 and 0.43–25 mg/L during winter and summer, respectively (**Figures 8A,B**). The high concentration of Br was located in the central part, characterized by a substantial seawater intrusion. The average concentration of Br in seawater

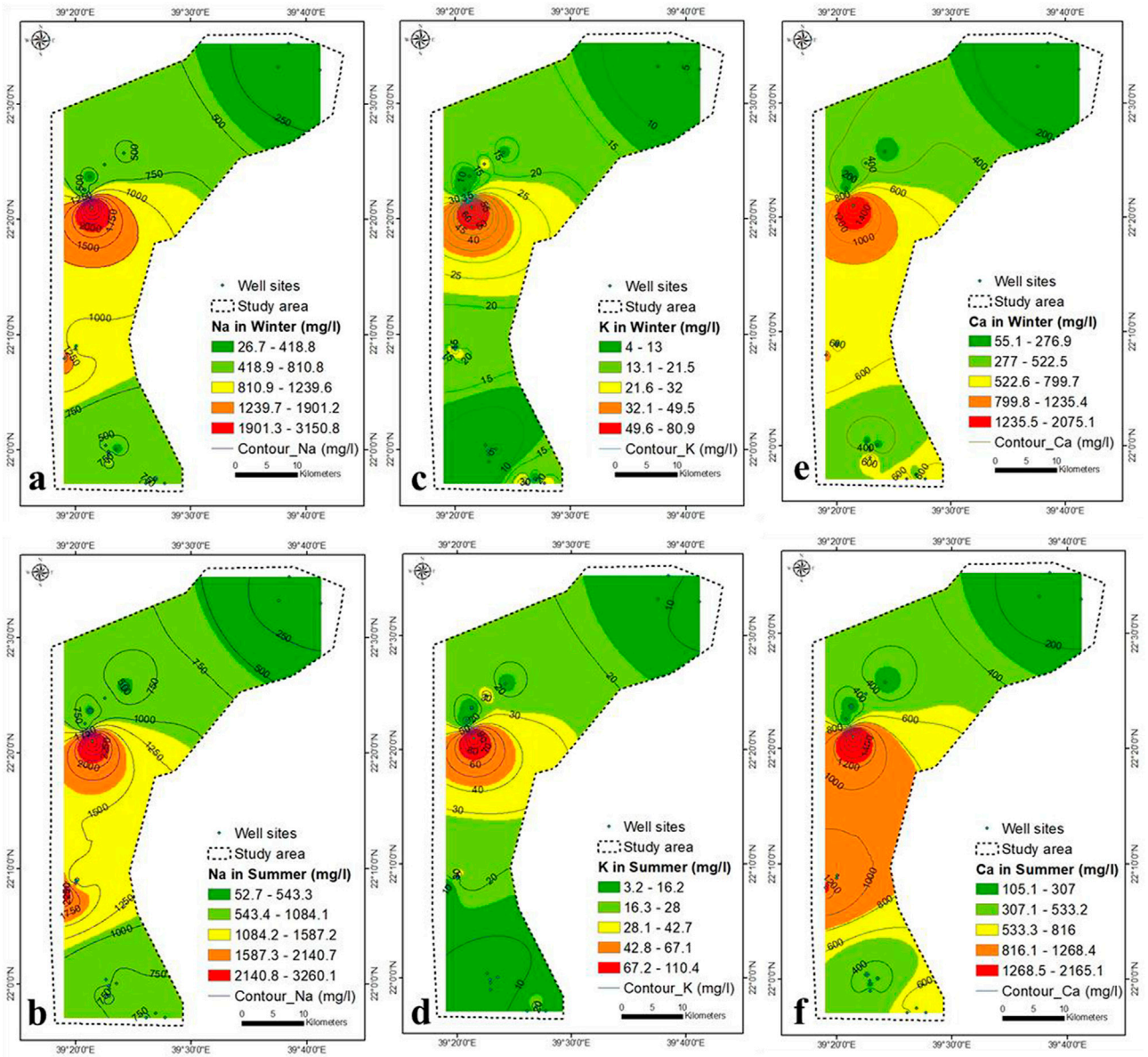

FIGURE 5 | Na **(A,B)**, K **(C,D)**, and Ca **(E,F)** concentration during winter and summer seasons (2021).

and freshwater is 65 and 0.5 mg/L, respectively. The NO_3^- concentration anomalies do not match Br anomalies, and negligible correlation analysis has been found between both (**Table 2** and **Supplementary Table S3**). The Br content is partly attributed to the contamination by fertilizer and sewage and is mainly caused by seawater intrusion. The Br concentration in summer was higher than in winter due to a higher rate of seawater intrusion, low recharge and higher pumping. A high concentration of F^- in the aquifer produces epidemiological effects (Edmunds and Smedley, 2005; Ozsvath, 2009). The concentration of F^- ranged from 1.4 to 1.9 mg/L during winter and summer, respectively, higher than the prescribed limits by WHO (maximum of 1.5 mg/L) (**Figures 8C,D**).

There is no association analysis between NO_3^- and F^- during winter and summer (**Table 2** and **Supplementary Table S3**). The F^--TDS correlation was strong within winter and summer (0.83 and 0.78, respectively). The F^- concentration is attributed to seawater intrusion and partially to anthropogenic sources.

The Al content is not toxic; however, a high concentration may produce coarse tremors, mental status deviations, speech disturbances, abnormal brain functioning and learning disabilities. In winter, the Al concentration ranged from 0.2 to 2.2 mg/L in lower central to southeastern parts, respectively (**Figure 8E**).

In winter, the correlation analysis between SO_4^- and Al was high (0.66) (**Table 2** and **Supplementary Table S3**), which

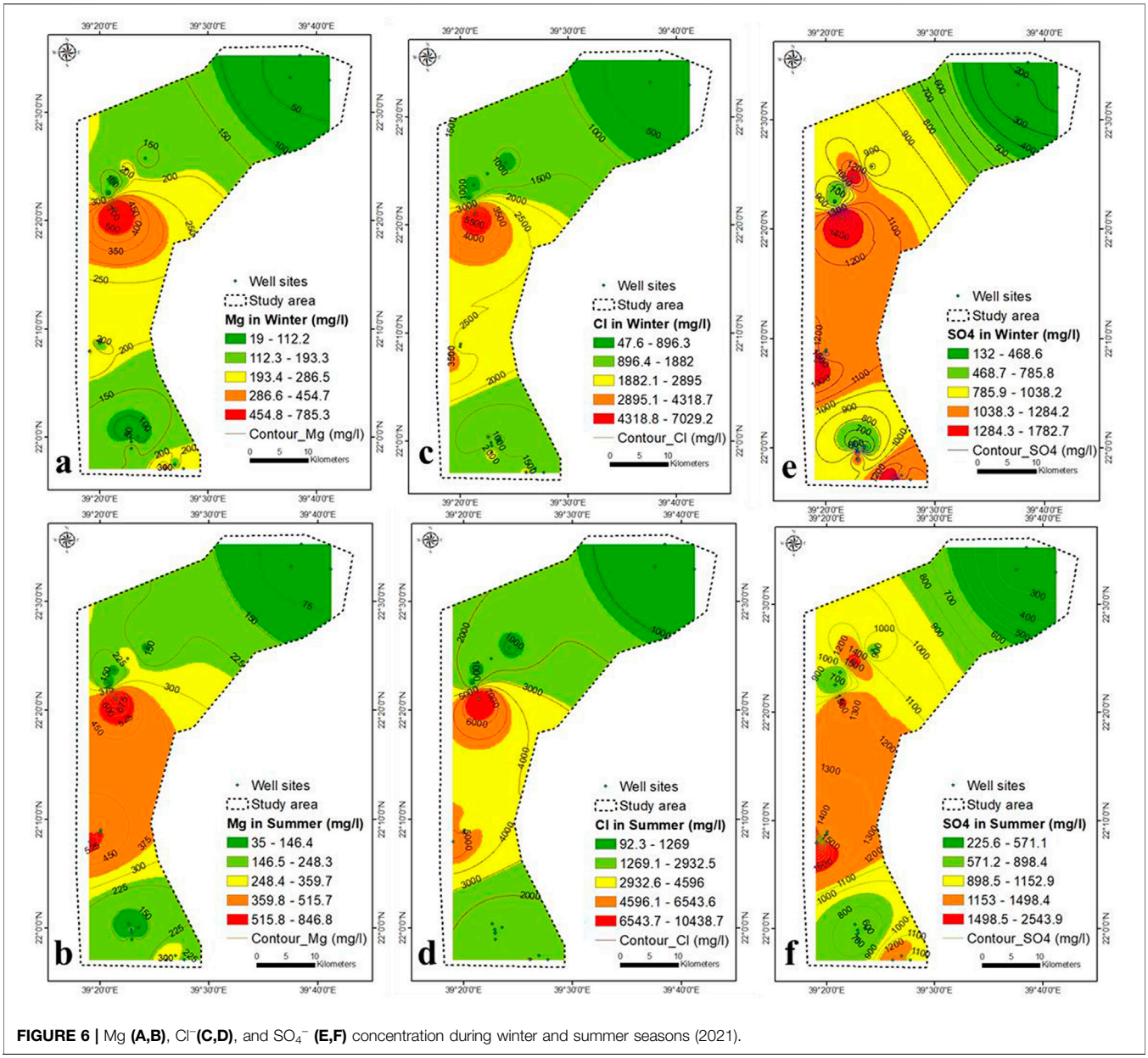

FIGURE 6 | Mg **(A,B)**, Cl^-**(C,D)**, and SO_4^- **(E,F)** concentration during winter and summer seasons (2021).

confirm the dissolution of sediments is the source of Al ions in the aquifer. The TDS-Al correlation was low (0.45), which indicate the main contribution for Al derived from the aquifer's sediments dissolution and partially from seawater intrusion. In summer, the Al concentration in the aquifer was below the detection limit, maybe diluted by higher aquifer salinity and precipitated by an increase in TDS concentration in summer.

The average B concentration in drinking and seawater was 0.5 and 2.4 mg/L, respectively (Weast, 1985; WHO, 2011). Soaps, detergents, bleaches, pesticides, fertilizers (borax), glass and flame retardants are made from B compounds. High B content impacts animals reproductively (USEPA, 2008; ISO 9390, 1990; Moss et al., 2003; WHO, 2011) and damages the brain, liver, stomach and kidneys.

The high B concentration in drinking water and irrigation water affects environmental health (Ravenscroft and McArthur, 2004). The B concentration ranged from 0.3 to 3 mg/L, increasing from lower central to southeastern parts (**Figure 8F**). The correlation analysis between B and Al was 0.77 (**Table 2**), showing that they are closely related. The concentration of B in groundwater was partly derived from seawater, aquifer dissolution and wastewater. The B concentration in summer was below the detection limit.

Cr concentrations ranged from 0.02 to 0.25 mg/L, following the same Al pattern (**Figure 8G**). Cr has a strong correlation with Al and B (0.97 and 0.77, respectively), but a weak correlation with TDS (0.41) (**Table 2** and **Supplementary Table S3**), implying that Cr is derived in part from aquifer dissolution, seawater, and

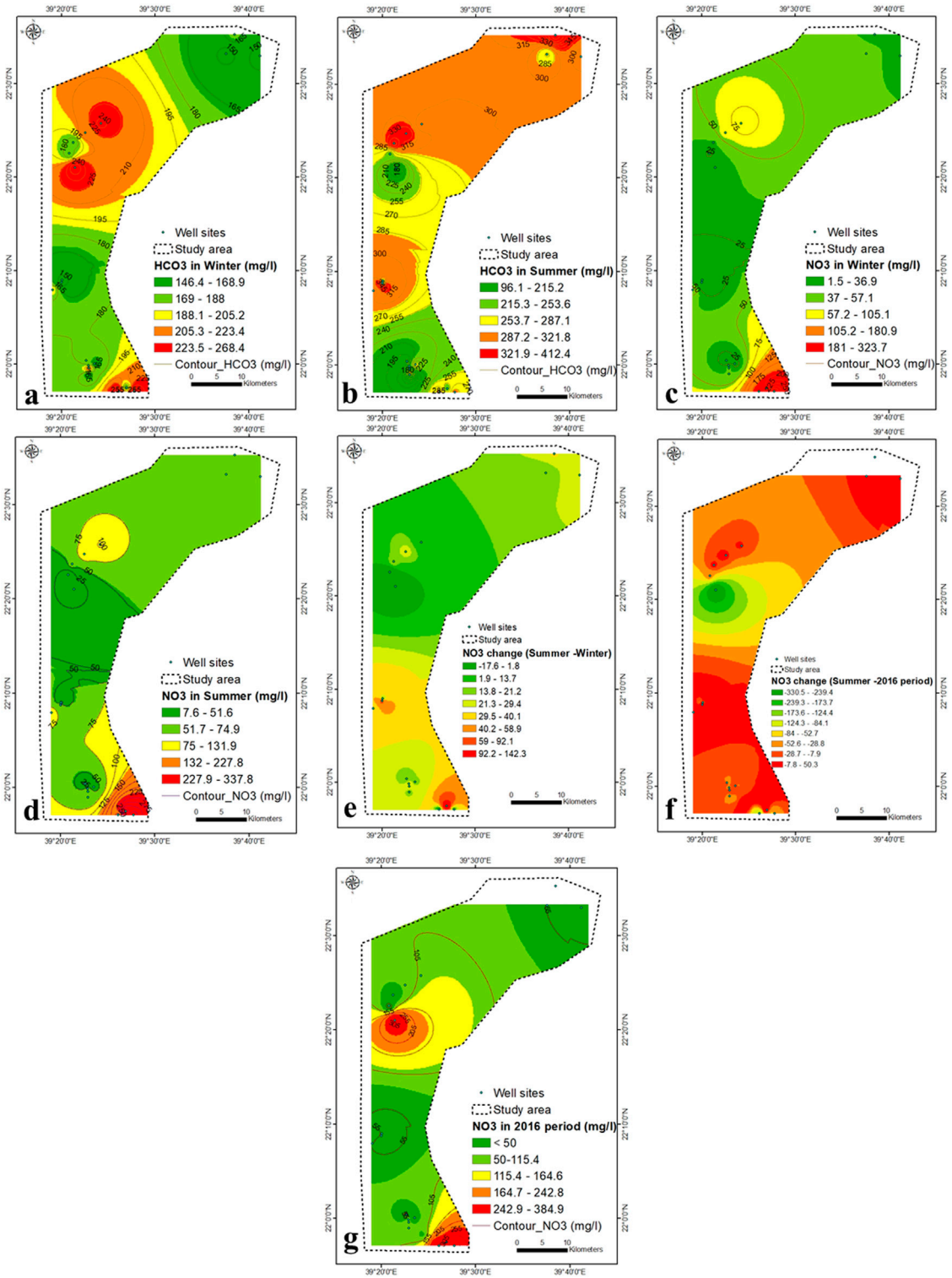

FIGURE 7 | (A–D) HCO_3^- and NO_3^- concentration within winter and summer seasons (2021), **(E)** variation in NO_3^- concentration in winter-summer **(F)** NO_3^- concentration in 2016 (Saleem and Algamal, 2016), **(G)** NO_3^- variation in summer of 2021 (this study) and 2016 (Saleem and Algamal, 2016).

agricultural wastewaters. The Cr concentration in summer was below the detection limit (<0.001 mg/L). The Ni concentration ranged from 0.01 to 0.22 mg/L in winter and increased from central to southeastern and from southeastern to northwestern parts (**Figure 8H**). The Ni is strongly correlated with Al, B, and Cr (0.92, 0.82, and 0.96), respectively. Ni is partially contributed

TABLE 2 | Pearson correlation analysis of the aquifer in winter 2021.

	pH	TDS	EC	Cl^-	NO_3–	SO_4^-	HCO_3^-	Na	K	Mg	Ca	Al	B	Ba	Co	Cr	Cu	Fe	Mn	Ni	Pb	Zn	F	Br
pH	1.00	–	–	–	–	–	–	–	–	–	–	–	–	–	–	–	–	–	–	–	–	–	–	–
TDS	−0.069	1.00	–	–	–	–	–	–	–	–	–	–	–	–	–	–	–	–	–	–	–	–	–	–
EC	−0.079	0.998**	1.00	–	–	–	–	–	–	–	–	–	–	–	–	–	–	–	–	–	–	–	–	–
Cl^-	−0.028	0.988**	0.980**	1.00	–	–	–	–	–	–	–	–	–	–	–	–	–	–	–	–	–	–	–	–
NO_3-	−0.098	0.08	0.12	−0.054-	1.00	–	–	–	–	–	–	–	–	–	–	–	–	–	–	–	–	–	–	–
SO_4^-	−0.152	0.835**	.852**	.759**	0.34	1.00	–	–	–	–	–	–	–	–	–	–	–	–	–	–	–	–	–	–
HCO_3	−.308	.527*	0.548*	0.42	0.574*	0.630**	1.00	–	–	–	–	–	–	–	–	–	–	–	–	–	–	–	–	–
Na	−.070	0.979**	0.968**	0.987**	−0.045-	0.732**	0.466*	1.00	–	–	–	–	–	–	–	–	–	–	–	–	–	–	–	–
K	−0.168	0.836**	0.828**	0.815**	0.14	0.607**	0.577**	0.863**	1.00	–	–	–	–	–	–	–	–	–	–	–	–	–	–	–
Mg	−0.077	0.955**	0.954**	0.930**	0.15	0.778**	0.597**	0.923**	0.871**	1.00	–	–	–	–	–	–	–	–	–	–	–	–	–	–
Ca	−0.043	0.981**	0.982**	0.970**	0.12	0.773**	0.518*	0.953**	0.832**	0.968**	1.00	–	–	–	–	–	–	–	–	–	–	–	–	–
Al	0.18	0.45	0.45	0.42	0.15	0.657**	0.14	0.34	0.11	0.36	0.38	1.00	–	–	–	–	–	–	–	–	–	–	–	–
B	0.15	0.24	0.23	0.22	0.08	0.457*	0.00	0.18	−.116-	0.09	0.13	.770**	1.00	–	–	–	–	–	–	–	–	–	–	–
Ba	0.04	0.37	0.37	0.34	0.22	0.529*	0.09	0.27	0.15	0.35	0.32	.800**	0.665**	1.00	–	–	–	–	–	–	–	–	–	–
Co	0.24	0.34	0.35	0.30	0.24	0.608**	0.06	0.23	−0.007	0.26	0.28	0.927**	0.793**	0.743**	1.00	–	–	–	–	–	–	–	–	–
Cr	0.18	0.41	0.41	0.37	0.19	0.637**	0.08	0.29	0.04	0.33	0.34	0.972**	0.765**	0.790**	0.972**	1.00	–	–	–	–	–	–	–	–
Cu	−0.012	0.630**	0.620**	0.648**	−0.157	0.569*	0.21	0.598**	0.37	0.531*	0.586**	0.742**	0.464*	0.569*	0.489*	0.646**	1.00	–	–	–	–	–	–	–
Fe	−0.068-	0.476*	0.484*	0.478*	−0.026-	0.491*	0.12	0.41	0.21	0.43	0.460*	0.726**	0.34	0.598**	0.513*	0.695**	0.888**	1.00	–	–	–	–	–	–
Mn	−0.010	0.35	0.33	0.39	−0.253	0.15	−0.050	0.44	0.547*	0.22	0.30	−0.006	−0.165	−0.106	−0.140	−0.117	0.24	0.03	1.00	–	–	–	–	–
Ni	0.25	0.32	0.32	0.28	0.23	0.593**	0.05	0.20	−0.031	0.24	0.25	0.923**	0.820**	0.745**	0.996**	0.962**	0.466*	0.474*	−0.155	−1.00	–	–	–	–
Pb	0.17	0.44	0.45	0.41	0.18	0.658**	0.12	0.33	0.09	0.36	0.38	0.990**	0.750**	0.802**	0.946**	0.991**	0.711**	0.747**	−0.074	−0.935**	1.00	–	–	–
Zn	0.23	0.23	0.24	0.18	0.32	.553*	0.12	0.11	−.022	0.18	0.15	.858**	.762**	.814**	.861**	.833**	0.39	0.40	−.154	−.880**	0.843**	1.00	–	–
F	−0.123	0.828**	0.806**	0.841**	−0.075-	0.484*	0.474*	0.884**	0.828**	0.879**	0.839**	0.06	−0.032	−0.09	0.00	0.05	0.37	0.22	0.22	−0.024	−0.07	−0.134	1.00	–
Br	−0.087	0.951**	0.952**	0.968**	−0.046	0.709**	0.38	0.947**	0.737**	0.883**	0.951**	0.33	0.16	0.28	0.22	0.30	0.609**	0.498*	0.31	0.19	0.34	0.08	0.802**	1.00

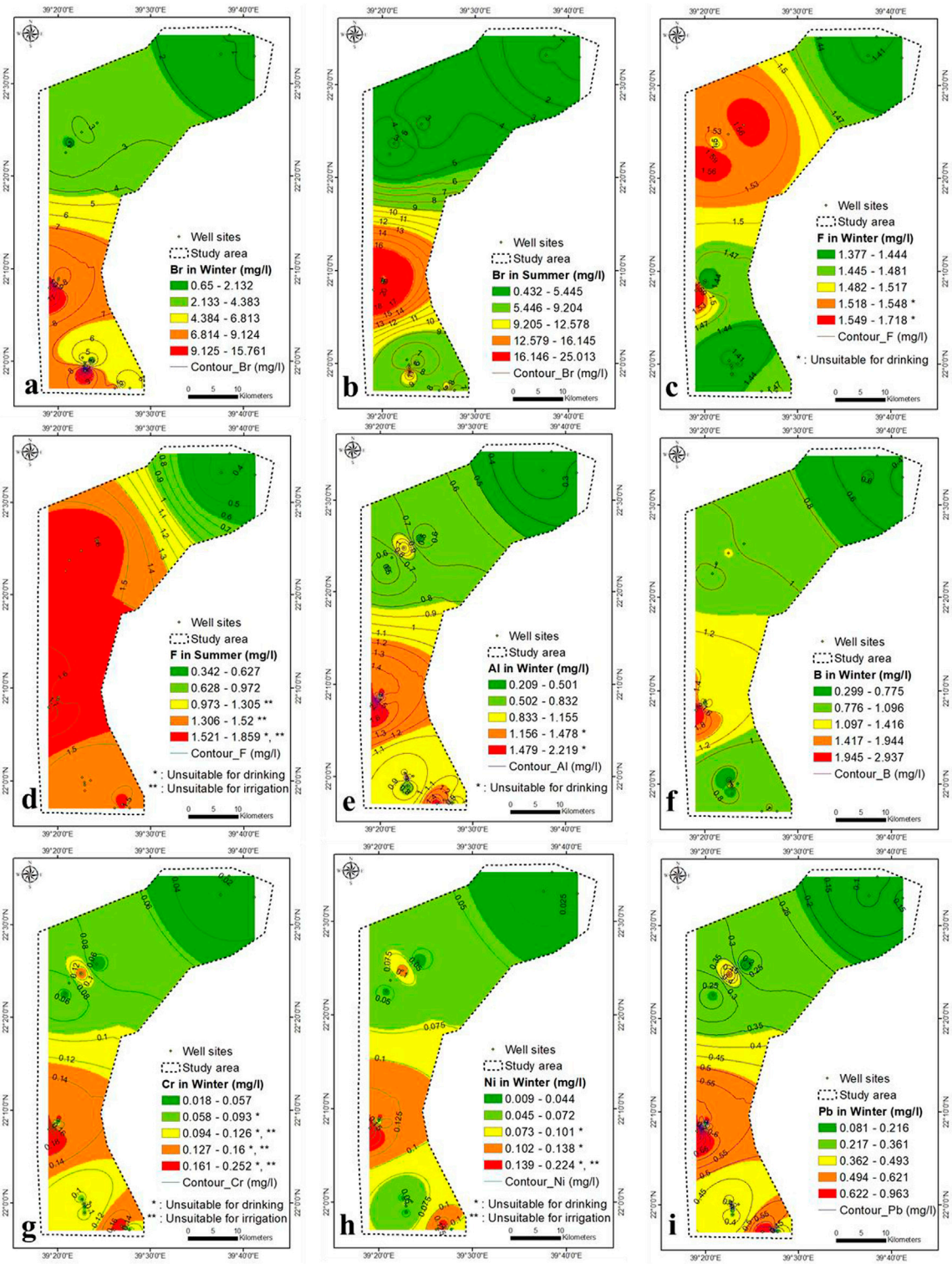

FIGURE 8 | (A–D) Br and F concentration in winter and summer seasons, respectively (2021), **(E–I)** Al, B, Cr, Ni and Pb concentration in winter, respectively (2021).

from seawater, fertilizers, and rock water interaction. The Ni content in the aquifer was lower than the detection limit in winter and summer (<0.001 mg/L).

Pb was toxic in connection with brain damage. It varied from 0.08 to 0.96 mg/L in winter and increased in the central northwest, and southeast parts (**Figure 8I**). Pb shows a strong

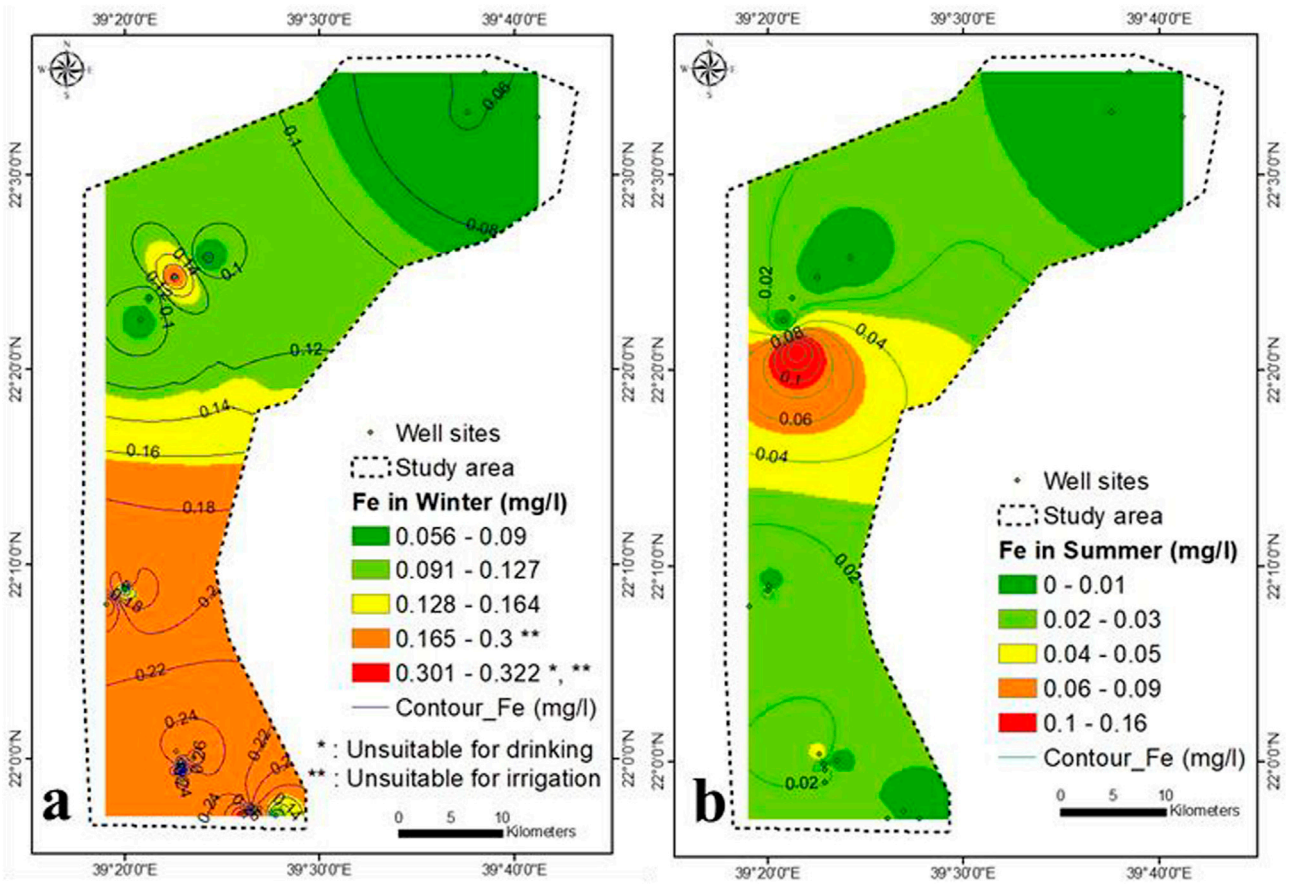

FIGURE 9 | Fe concentration in winter **(A)** and summer **(B)** (2021).

correlation with SO_4^-, Al, B, Cr, Fe and Ni (0.66, 0.99, 0.75, 0.99, 0.75 and 0.94, respectively) and might be attributed to the dissolution of geomedia, seawater and wastewater. Phosphate and superphosphate fertilizers contain impurities such as Pb in the manufacture of fertilizers. The Pb concentration summer was below the detection limit (<0.001 mg/L).

In winter, the Fe concentration increases in the southeastern and northwestern parts (>0.3 mg/L) (**Figure 9A**), which is more than the prescribed drinking guidelines (WHO, 2017). Fe is strongly correlated with Al and Cr (0.73 and 0.70, respectively) and weakly correlated with TDS (0.48), confirming that the iron content partly contributed to the geomedia dissolution, seawater, and wastewaters. The Fe concentration in summer was diluted and was lower than that in winter (range from below the detection limit to 0.16 mg/L), which might be related to the co precipitated with increasing TDS concentration in summer (**Figure 9B**).

The Se concentration ranged from below the detection limit (<0.001) to 0.063 mg/L in summer and increased from the north to the southeast (**Figure 10A**). The Se is correlated with SO_4^- (r = 0.58), indicating the dissolution of geomedia rather than anthropogenic sources. The concentration of Sr in groundwater samples is greater than 1.5 mg/L throughout the study area in summer, which enhance the negative health impact (**Figure 10B**). Its concentration is increased in the central part (5.7–21.7 mg/L), indicating the source of seawater intrusion. Sr is strongly correlated to TDS, Cl, Na, Mg, and Ca (0, 99, 0.98, 0.97, 0.97 and 0.980, respectively), confirming that Sr is mainly supplied by seawater. According to the United States Environmental Protection Agency (USEPA, 2014), the permissible Sr limit in drinking water is 1.5 mg/L. The Ba concentration in winter varied from 0.061 to 0.24 mg/L (**Figure 10C**), and reflect no pollution with respect to Ba (<0.7 mg/L).

A high concentration of Cd and Co caused vomiting, nausea, kidney failure, irritability, insomnia, headache, hypersalivation, choking, chest pain, diarrhoea, abdominal pain, dry throat, blisters, pneumonia and cough (https://www.health.state.mn.us). In winter, the Cd and Co concentration ranged from below the detection limit to 0.055 mg/L and 0.003–0.14 mg/L, respectively (**Figures 10D,E**). They increased in the central part and from north to south. It may be due to anthropogenic sources, particularly fertilizers (as impurities present in the fertilizer during manufacturing) and septic tanks. In summer, Cd and Co levels were below the detection limit (<0.001 mg/L). Co is strongly correlated to Al, B and Ba (0.93, 0.97 and 0.74, respectively) in winter and

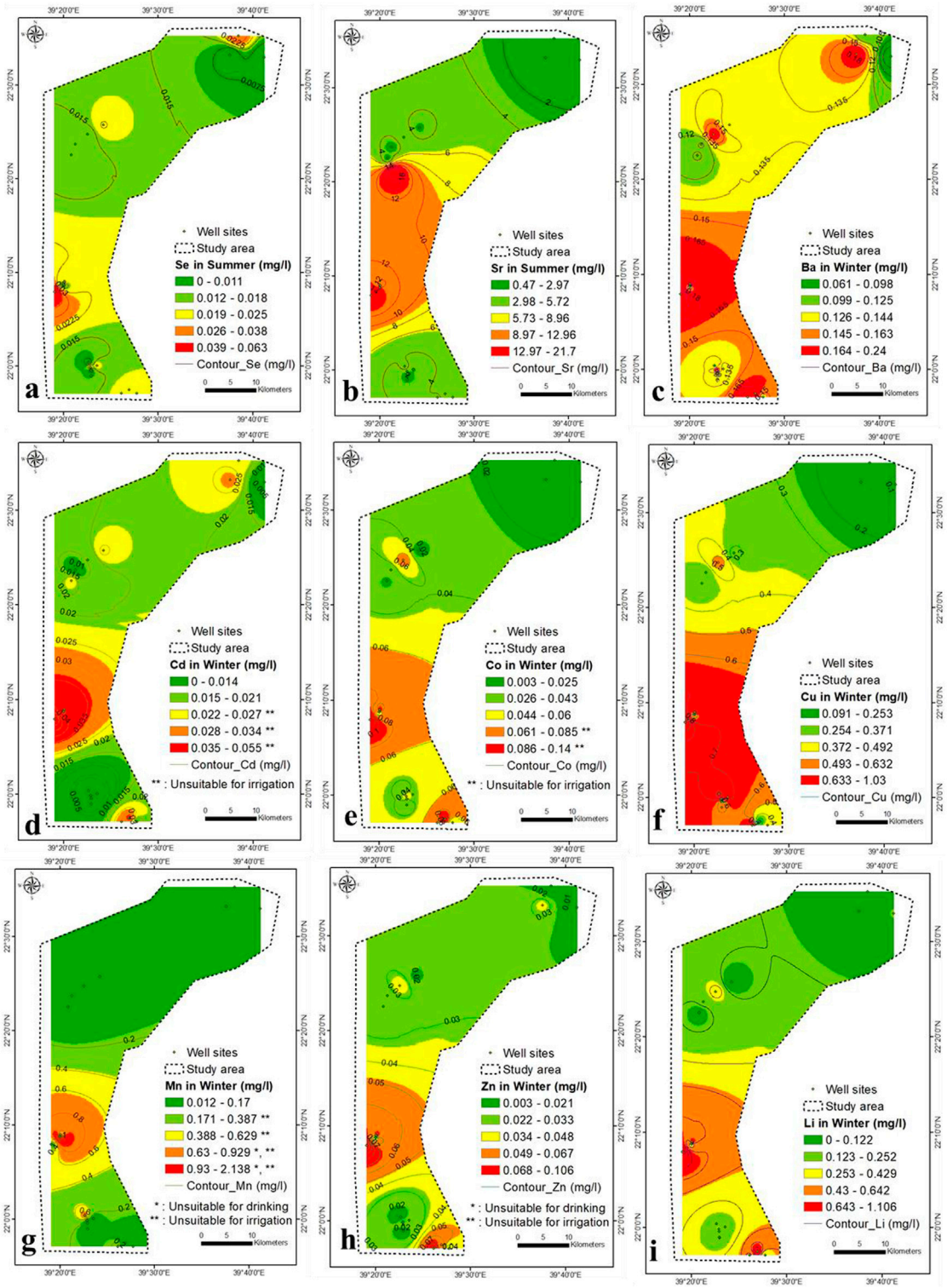

FIGURE 10 | (A–I) Se, Sr, Ba, Cd, Co, Cu, Mn, Zn and Li concentration in groundwater (2021).

moderately related to SO_4^- (0.61). Cd and Co have partly contributed to the dissolution of geomedia and agricultural wastewater.

In winter, the Cu concentration ranged from 0.09 to 1.03 mg/L (**Figure 10F**) and increased mainly towards the southern region. The Cu is moderately correlated with TDS, Cl, SO_4^-, Na, Mg, Ca,

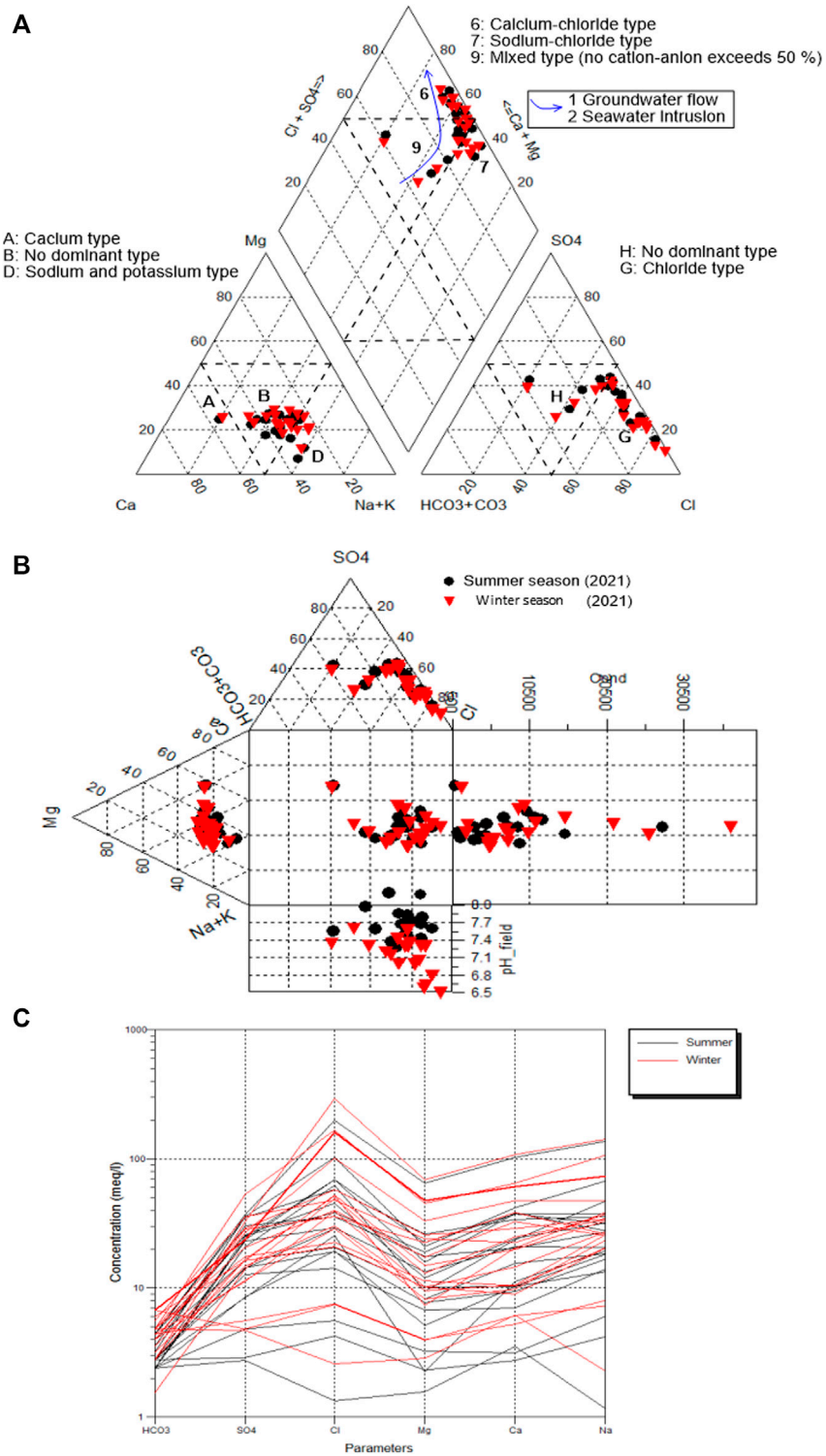

FIGURE 11 | (A) Piper, **(B)** Durov, and **(C)** Schoeller diagrams of groundwater.

B, Ba, Co, and Cr (0.63, 0.65, 0.57, 0.60, 0.53, 0.59, 0.46, 0.57, 0.49, and 0.65, respectively), and strongly correlated with Al (0.74), confirming its contribution by aquifer sediments dissolution and partially from anthropogenic sources. The high concentration of Cu causes vomiting, diarrhoea, stomach cramps, nausea, liver damage, and kidney disease (https://www.health.state.mn.us).

High Mn concentration in drinking water can be harmful to health. Water with dissolved Mn concentration can discolor cloth, if used for washing, cause scaling in water lines, and make the water look, smell, or taste bad (https://www.health.state.mn.us). The concentration of Mn in winter ranged from 0.012 to 2.14 mg/L (**Figure 10G**) and increased in the central part. The Mn correlation with K (0.55), indicating that both elements are partially derived from rock water interaction. The Cu and Mn concentration were below the detection limit (0.001 mg/L) in summer.

The Zn and Li concentrations ranged from 0.003 to 0.106 mg/L and below the detection limit to 1.106 mg/L in winter, which shows no pollution due to their low concentrations, whereas in summer, Zn and Li were below the detection limit (<0.001 mg/L) (**Figures 10H,I**). Be, Mo, Sb, Ti and PO_4 were below the detection limit (<0.001 mg/L), which can be attributed to the increase in bacteria and viruses in the summer. The latter absorbs these toxic metals from the aquifer.

3.2 Hydrochemical Facies

Due to aquifer sediments, seawater intrusion, and anthropogenic influence, water flowing through an aquifer takes on specific chemical compositions. The facies are a function of the lithology, solution kinetics, and flow patterns of the aquifer. Piper's Trilinear Diagram (Piper, 1953) classified hydrochemical facies based on dominating ions (**Figure 11A**). Distinct hydrochemical zonation is differentiated into many varieties in the winter and summer seasons, as indicated in **Supplementary Table S4**.

It is evident from **Figure 11A** that the majority of groundwater samples were found in fields 6 and 9, which exhibited $CaCl_2$ and mixed water, respectively. The samples in field seven are of NaCl type. Durov (1948) validated the Piper diagram and clarified the hydrogeochemical processes in the aquifer system (**Figure 11B**). The Schoeller plot (Schoeller, 1977) reveals that the groundwater has high levels of Cl and Na (**Figure 11C**). There is evidence of anthropogenic activities, seawater intrusion, and lithogenic sources. Changes in water types were observed in the Schoeller diagram due to rock water interaction of varied geology, fertilizers, and rainfall infiltration.

3.3 Ionic Correlation, Compositional Variation, and Seawater Intrusion Rate

TDS has a significant correlation with Cl^- ($R^2 = 0.94$), indicating the process of seawater intrusion (**Supplementary Figure S5A**). Cl^- is strongly correlated with cations such as Na, Ca, Mg, and K have substantial correlations (R^2 = 0.97, 0.94, 0.87, and 0.66, respectively, which revealed that seawater intrusion played a major role in aquifer hydrogeochemistry (**Supplementary Figure S5B–D**). It is because Cl^- was a conservative ion in saltwater. (De Montety et al., 2008; Sun et al., 2017). The moderate correlations between Cl^--SO_4^- and Cl^--K (R^2 = 0.58 and 0.66, respectively), suggest that rock water interaction and seawater intrusion play a role (**Supplementary Figures S5E,F**).

The chemical concentrations during the winter and summer seasons show that Na > Ca > Mg > K and $Cl^- > SO_4^- > HCO_3^-$ (**Figures 12A,B**). To analyze the freshwater/seawater interface, the Simpson's ratio was calculated [r Cl^-/r (HCO_3^- + CO_3)] (**Figures 12C,D**) (Singaraja et al., 2013). **Figures 12C,D** show the distribution rate of seawater intrusion. The central part has the highest rate of seawater intrusion, which was attributed to open Wadis that were not blocked by hard rocks (**Supplementary Figure S2**). The lowest rates were seen in the northeastern and southeastern sections of the country (**Figures 12C,D**), caused by hard rocks limiting seawater intrusion due to low permeability characteristics.

3.4 Saturation Index

The calcite or dolomite saturation index is near or above zero or the equilibrium line and is mainly affected by seawater intrusion and partly by geomedia dissolution (**Figures 13A,B**). During the winter and summer, most water samples appear to be in equilibrium or supersaturated with the calcite and dolomite minerals (**Figures 13C,D**), indicating that both minerals are present in the aquifer when TDS is greater to seawater intrusion and rock-water interaction. Calcite and dolomite saturation indices are generally related to TDS concentrations. The index of gypsum saturation in the collected groundwater samples increase with increasing sulphate concentrations (**Figures 13E,F**). Gypsum tends to dissolve in water that is not saturated concerning gypsum. **Figures 13G,H** shows how the structure is simply progressing towards equilibrium concerning the minerals available for dissolution (e.g., calcite and dolomite).

3.5 Granulometric Analysis

The gravel and sand distribution of soil samples are high overall in the study area, while clay percent increases towards the northeastern part (**Figures 14A–C**). The majority of the studied area has soil hydraulic conductivity (K) of more than 5 m/d, attributed to sand with the largest particle size concentration (**Figure 14D**). It reflects a high to very high recharge of the aquifer by infiltration precipitation. Most of the samples are gravel sand followed by sand gravel (**Supplementary Figures S6, S7**; **Supplementary Table S5**).

3.6 Water Quality for Drinking and Irrigation Purposes

3.6.1 Drinking and Irrigation Purposes Based on Toxic Metals

The southeastern and spotted northern parts were unsuitable for drinking (NO_3^- > 45 mg/L), while the rest was suitable (**Figures 7C,D** and **Supplementary Table S6**). The groundwater samples were unsuitable for drinking purpose with respect to Br (>0.5 mg/L), Cr (>0.1 mg/L), Pb (>0.01 mg/L), Se (>0.02 mg/L), Sr (>1.5 mg/L), and Cd (>0.002 mg/L) (**Figures 8A**,**B**,G,I, **10A**,**B**,D), respectively. In the winter season, the northeastern and southeastern parts were unsuitable for drinking (F < 1.5 mg/L), whereas southern part was unsuitable for drinking (Fe > 0.2 mg/L) (**Figures 8C**, **9A**), respectively. In summer season, the

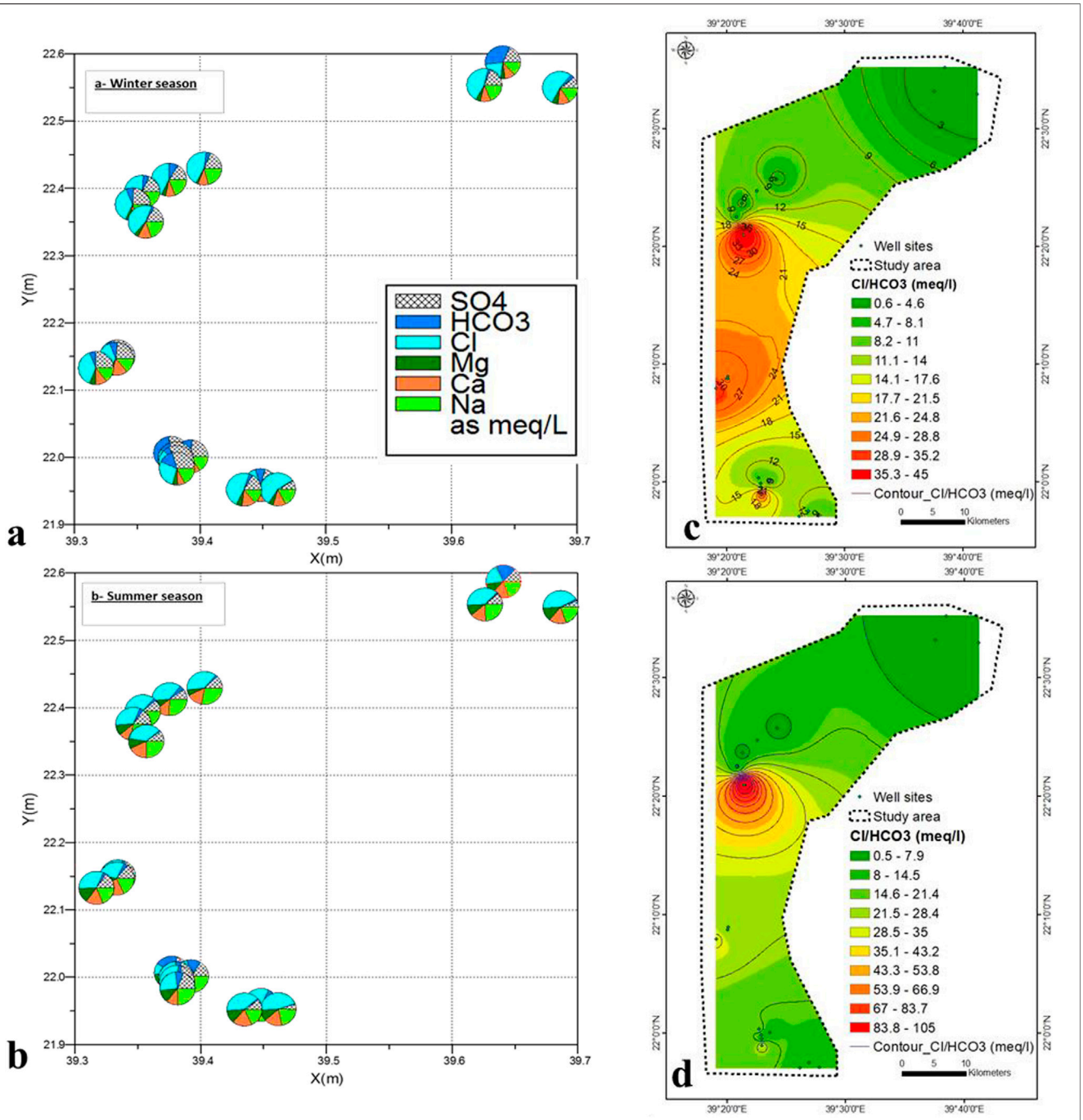

FIGURE 12 | (A,B) Variation of groundwater samples by Pie diagram in winter and summer season, **(C,D)** Seawater intrusion rate in winter and summer seasons.

western part was unsuitable for drinking (F < 1.5 mg/L), the samples were suitable with respect to Fe (<0.2 mg/L) (**Figures 8D**, **9B**), respectively. The lower central and southeastern parts were unsuitable for drinking (Al > 1 mg/L) (**Figure 8E**). The samples spotted through northern and southern parts were unsuitable for drinking (Ni > 0.02–0.07 mg/L) (**Figure 8H**). Fewer samples in central part were unsuitable for drinking (Mn > 0.5 mg/L) (**Figure 10G**). The silver (Ag) concentration shows some samples higher than the drinking guideline (0.1 mg/L) (**Supplementary Figure S8**). The aquifer samples were suitable for drinking application with respect to B (<2.4 mg/L), Ba (<0.7 mg/L), Co (<2 mg/L), Cu (<2 mg/L), Zn (<3 mg/L), and Li (<2.5 mg/L) (**Figures 8F**, **10C–F–F**,H,I), respectively. The NO_2 and V concentration ranged from (<0.001–3) and (<0.001–0.025 mg/L) within winter and summer,

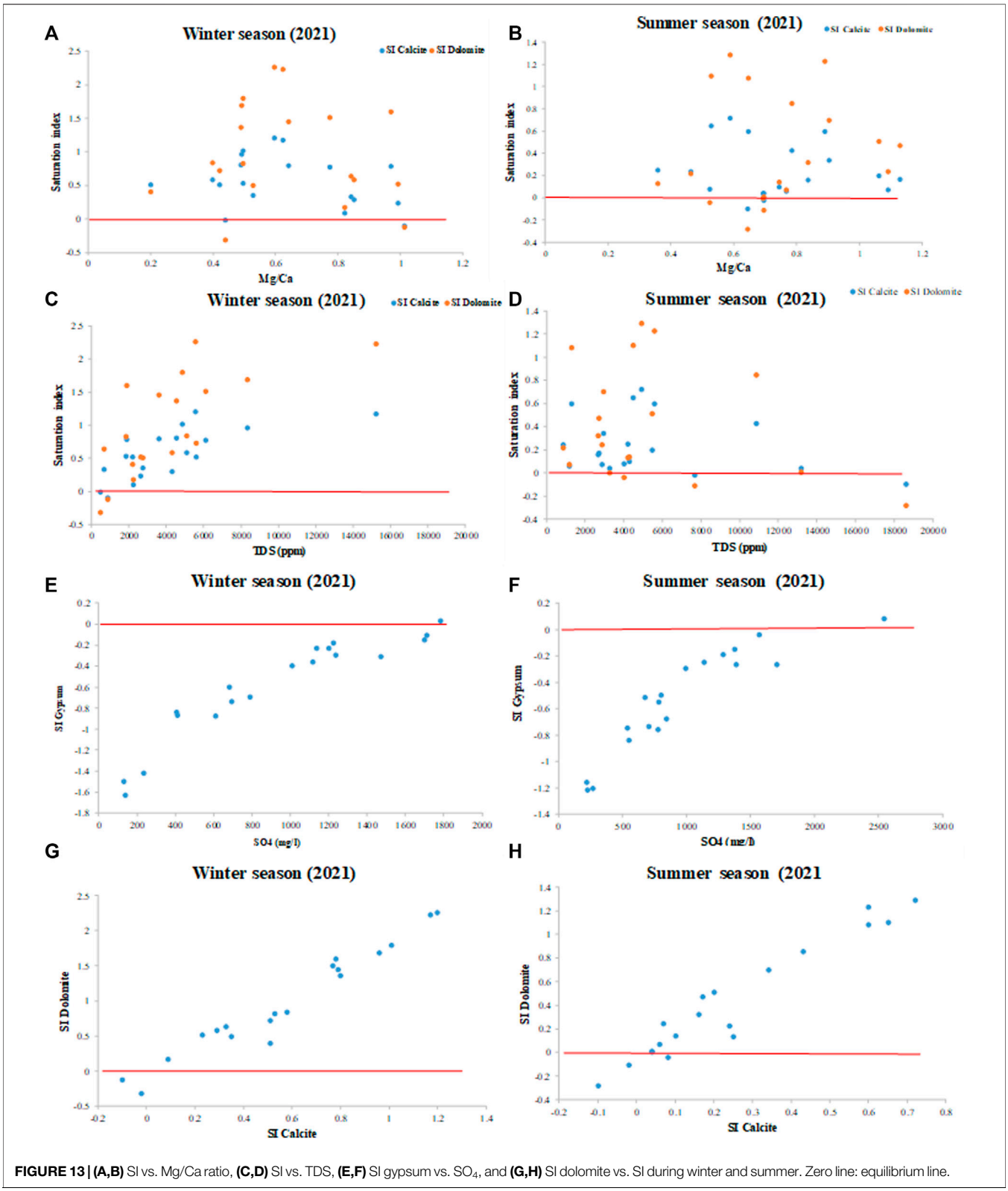

FIGURE 13 | (A,B) SI vs. Mg/Ca ratio, **(C,D)** SI vs. TDS, **(E,F)** SI gypsum vs. SO_4, and **(G,H)** SI dolomite vs. SI during winter and summer. Zero line: equilibrium line.

respectively. The samples have NO_2 concentration higher than 0.9 mg/L was unsuitable for drinking, while all samples was suitable with respect to V (<0.1 mg/L).

Most of the groundwater samples was unsuitable for irrigation purpose with respect to B (>0.5 mg/L), Cr (>0.1 mg/L), Fe (>0.2 mg/L), Se (>0.02 mg/L), Cd (>0.01 mg/L), Co (>0.05 mg/

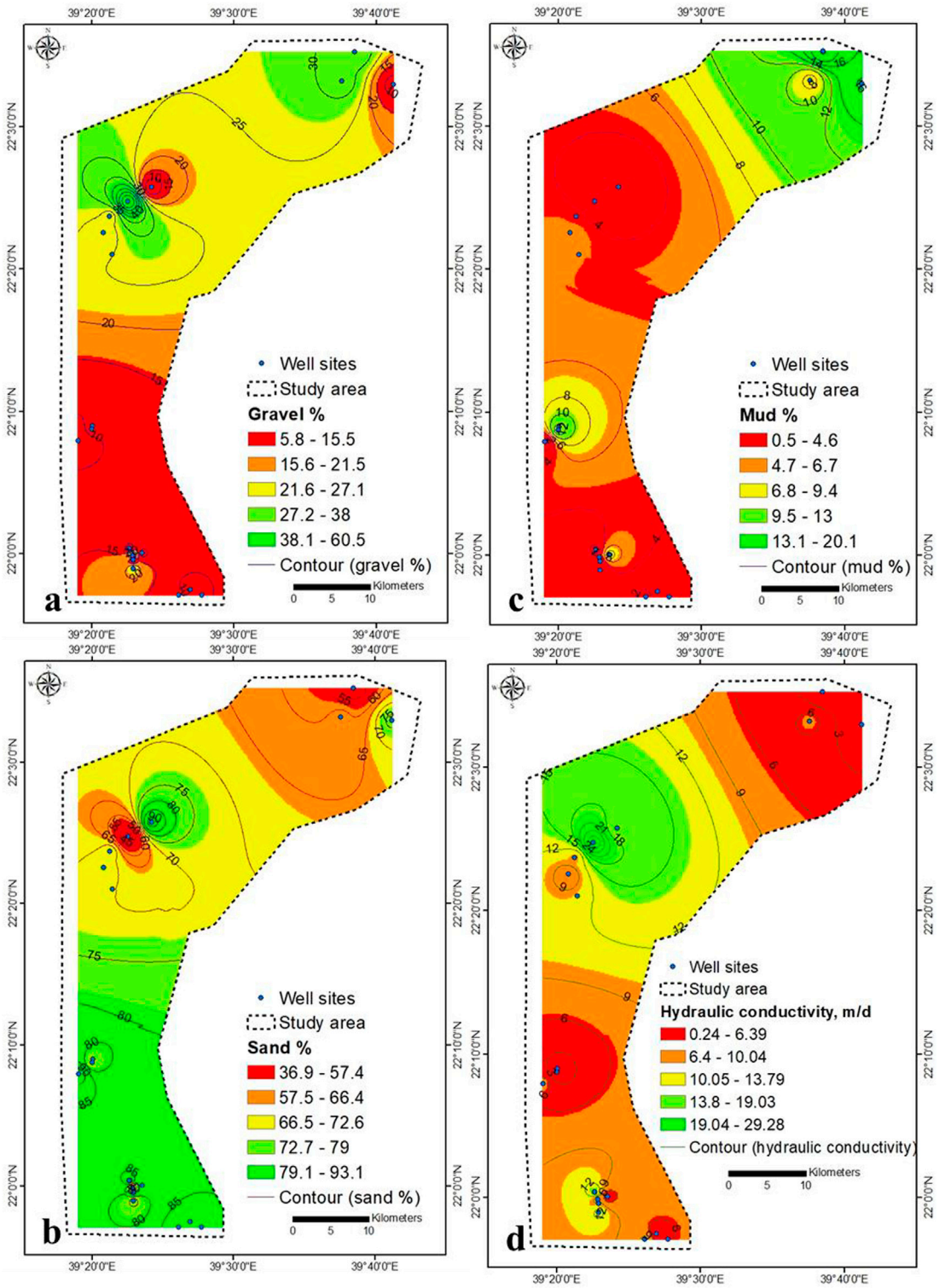

FIGURE 14 | Granulometric investigation **(A–C)** and hydraulic conductivity **(D)** of top soil.

L), Cu (>0.2 mg/L), and Mn (>0.2 mg/L), and (**Figures 8F**,G, **9A**, **10A**,**D–G–G**), respectively. All groundwater samples were unsuitable for irrigation in winter, while in summer most of the samples were unsuitable for irrigation with respect to F (F > 1 mg/L) (**Figures 8C,D**). The aquifer samples were suitable for irrigation application with respect to Al (<5 mg/L), Ni (<0.2 mg/

L), Pb (<2 mg/L), Fe (<0.2 mg/L), and Zn (<2 mg/L) (**Figures 8E**,H,I, **9B**, **10H**), respectively.

3.6.2 US Salinity Laboratory's Salinity Hazards Map

The high concentration of TDS in the aquifer results in osmotic pressure in the soil solution. At the same time the Na is incorporated into the lattices (cation exchange), resulting in lower K. As a result, the water barely reaches the plant's root, which reduces crop growth. The EC-SAR illustration shows an aquifer irrigation application. The SAR was estimated by dividing the Na concentration by the Ca and Mg concentration (meq/l) (Kalra and Maynard, 1991). The Na is absorbed by the soil, fills the pore spaces in the soil, and causes a decrease in permeability. Thus, they retard crop productivity and deterioration of agricultural products. It is clear from the classification of groundwater samples based on the SAR (Todd, 1959) that most of the samples belong to classes C4S1, C4S2, C4S3 and C4S4 (SAR > 10), which are considered unsuitable for irrigation. (Richards, 1954). (**Supplementary Figure S9**). Fewer samples belong to the high salinity/low Na type (C3S1).

4 CONCLUSIONS AND RECOMMENDATIONS

Groundwater chemistry in the Khulais region is dominated by natural processes rather than anthropogenic activity. Seawater intrusion, rock-water interaction, groundwater movement, and evaporation are critical natural processes influencing groundwater chemistry. In contrast, agricultural wastewater is the predominant source of anthropogenic contamination. High amounts of EC, TDS, and Cl are linked to seawater intrusion in the central section. TDS levels were higher in the summer than in the winter. The TDS during summer in this study (2021) also shows an increasing pattern compared to the TDS during summer in 2016. High NO_3^- and Sr levels are caused by agricultural wastewaters and seawater intrusion, respectively.

Most samples were unsuitable for drinking and irrigation purposes, based on Br, F, and Fe concentration within winter and summer seasons. Few samples were inappropriate for drinking and irrigation purposes based on Al, Cr, B, Ni, Pb, Cd, Co, Cu, and Mn concentrations in winter; however, in summer, Al, Cr, Pb, Cd, Co, Cu, Mn, Zn, Li, Be, Mo, Sb, Li, and PO4 concentrations were very low (0.001 mg/L). The majority of the groundwater samples were unsuitable for irrigation purposes based on EC and SAR values. The unconfined aquifer promotes anthropogenic sources of pollution. The majority of the region under investigation had been swamped by seawater. Temperature changes, rainfall fluctuations, seawater intrusion, and anthropogenic sources influence groundwater pollution, resulting in a drop in groundwater quantity and quality. Proper treatment is needed to eliminate the concentration of the toxic metal in the groundwater. Groundwater resource management and planning, emphasising seawater intrusion, must be systematic and based on hydrogeochemical outputs.

DATA AVAILABILITY STATEMENT

The original contributions presented in the study are included in the article/**Supplementary Material**, further inquiries can be directed to the corresponding author.

AUTHOR CONTRIBUTIONS

MYAK is the principal and corresponding author of the manuscript. MYAK and ME contributed to the concept and modification of the manuscript. MYAK, ME, WG, and AA help in the collection and analysis of the data. AMS and AK reviewed and revised the manuscript. All authors approved the publication of the final manuscript.

FUNDING

This research was funded by Institutional Funds Projects under grant no. (IFPRC-098-145-2020). Therefore, the authors gratefully acknowledge technical and financial support from the Ministry of Education and King Abdulaziz University, Jeddah, Saudi Arabia.

ACKNOWLEDGMENTS

This research was funded by Institutional Funds Projects under Grant No. (IFPRC-098-145-2020). Therefore, the authors gratefully acknowledge technical and financial support from the Ministry of Education and King Abdulaziz University, Jeddah, Saudi Arabia.

SUPPLEMENTARY MATERIAL

The Supplementary Material for this article can be found online at: https://www.frontiersin.org/articles/10.3389/fenvs.2021.800517/full#supplementary-material

REFERENCES

Abderrahman, W. A. (2006). *Groundwater Resources Management in Saudi ArabiaSpecial Presentation at Water Conservation Workshop*. Khober, Saudi Arabia.

Adimalla, N., and Li, P. (2018). Occurrence, Health Risks, and Geochemical Mechanisms of Fluoride and Nitrate in Groundwater of the Rock-Dominant Semi-arid Region, Telangana State, India. *Hum. Ecol. Risk Assess. Int. J.* 25, 81–103. doi:10.1080/10807039.2018.1480353

Adimalla, N., and Qian, H. (2019). Groundwater Quality Evaluation Using Water Quality index (WQI) for Drinking Purposes and Human Health Risk (HHR)

Assessment in an Agricultural Region of Nanganur, South India. *Ecotoxicology Environ. Saf.* 176, 153–161. doi:10.1016/j.ecoenv.2019.03.066

Al-Ibrahim, A. A. (1991). *Excessive Use of Groundwater Resources in Saudi Arabia: Impacts and Policy Options*. Ambio, 34–37.

Alcamo, J., Henrichs, T., and Rösch, T. (2000). *World Water in 2025: Global Modeling and Scenario Analysis for the World Commission on Water for the 21st century, Kassel World Water Ser Rep 2*. Kassel, Germany: Cent for Environ Syst Res, Univ of Kassel.

Allen, D. M., and Suchy, M. (2001). Geochemical Evolution of Groundwater on Saturna Island, British Columbia. *Can. J. Earth Sci.* 38, 1059–1080. doi:10.1139/e01-007

APHA (1998). *Standard Methods for the Examination of Water and Wastewater*. 20th edn. Washington, DC: American Public Health Association.

Bazuhair, A. S., Hussein, M. T., Alyamani, M. S., and Ibrahim, K. (1992). *Hydrogeophysical Studies of Khulais basin, Western Region, Saudi Arabia*. Saudi Arabia: Unpub. Report, King Abdulaziz Uni, Jeddah.

Behera, A. K., Chakrapani, G. J., Kumar, S., and Rai, N. (2019). Identification of Seawater Intrusion Signatures through Geochemical Evolution of Groundwater: a Case Study Based on Coastal Region of the Mahanadi delta, Bay of Bengal, India. *Nat. Hazards* 97 (3), 1209–1230. doi:10.1007/s11069-019-03700-6

Chen, J., Wu, H., and Qian, H. (2016). Groundwater Nitrate Contamination and Associated Health Risk for the Rural Communities in an Agricultural Area of Ningxia, Northwest China. *Expo. Health* 8 (3), 349–359. doi:10.1007/s12403-016-0208-8

De Montety, V., Radakovitch, O., Vallet-Coulomb, C., Blavoux, B., Hermitte, D., and Valles, V. (2008). Origin of Groundwater Salinity and Hydrogeochemical Processes in a Confined Coastal Aquifer: Case of the Rhône delta (Southern France). *Appl. Geochem.* 23, 2337–2349. doi:10.1016/j.apgeochem.2008.03.011

Durov, S. A. (1948). Natural Waters and Graphic Representation of Their Compositions. *Dokl Akad Nauk SSSR* 59, 87–90.

Edmunds, W. M., and Smedley, P. L. (2005). *Fluoride in Natural Waters Essentials of Medical Geology*. Editors B. J. Alloway and O. Selinus, 301–329.

Fekkoul, A., Yassine, Z., Mimoun, B., Alae-eddine, B., Abdelhakim, J., and Salem, B. (2013). *Impact of Anthropogenic Activities on the Groundwater Resources of the Unconfined Aquifer of Triffa plain*. Eastern Morocco Arab.

Ferguson, G., and Gleeson, T. (2012). Vulnerability of Coastal Aquifers to Groundwater Use and Climate Change. *Nat. Clim. Chag* 2, 42–345. doi:10.1038/nclimate1413

Food and Agriculture Organization (Fao) of the United Nations (2009). *Groundwater Management in Saudi Arabia*. Rome: Draft synthesis report, 14.

Gabr, S. S., Morsy, E. A., El Bastawesy, M. A., Habeebullah, T. M., and Shaaban, F. F. (2017). Exploration of Potential Groundwater Resources at Thuwal Area, north of Jeddah, Saudi Arabia, Using Remote Sensing Data Analysis and Geophysical Survey. *Arabian J. Geosciences* 10 (23), 1–19. doi:10.1007/s12517-017-3295-3

Han, D. M., Song, X. F., Currell, M. J., Yang, J. L., and Xiao, G. Q. (2014). Chemical and Isotopic Constraints on Evolution of Groundwater Salinization in the Coastal plain Aquifer of Laizhou Bay, China. *J. Hydrol.* 508, 12–27. doi:10.1016/j.jhydrol.2013.10.040

Hazen, A. (2013). *XXIII. Some Physical Properties of Sands and Gravels, With Special Reference to their use in Infiltration. In State Sanitation: A Review of the Work of the Massachusetts State Board of Health, Volume II*. Harvard University Press, 232–248.

Hussein, M., Bazuhair, A., and Al-yamani, M. (1993). Groundwater Availability in the KhulaisPlain, Western Saudi Arabia. *Hydrological Sci. -Journal- des Sci. Hydrologiques* 3S (3), 6–1993. doi:10.1080/02626669309492663

ISO 9390 (1990). *Water Quality Determination of Borate Spectrometric Method Using Azomethine-H*. Geneva: International Organization for Standardization.

Jalali, M. (2011). Nitrate Pollution of Groundwater in Toyserkan, Western Iran. *Environ. Earth Sci.* 62 (5), 907–913. doi:10.1007/s12665-010-0576-5

Kalra, Y. P., and Maynard, D. G. (1991). *Methods Manual for forest Soil and Plant Analysis. Information Report NOR-X-319. Northwest Region, Northern Forestry Centre, Forestry Canada*.

Khan, M. Y. A., and Wen, J. (2021). Evaluation of Physicochemical and Heavy Metals Characteristics in Surface Water under Anthropogenic Activities Using Multivariate Statistical Methods, Garra River, Ganges Basin, India. *Environ. Eng. Res.* 26 (6), 200280. doi:10.4491/eer.2020.280

Khan, M. Y. A., ElKashouty, M., and Bob, M. (2020). Impact of Rapid Urbanization and Tourism on the Groundwater Quality in Al Madinah City, Saudi Arabia: a Monitoring and Modeling Approach. *Arabian J. Geosciences* 13 (18), 1–22. doi:10.1007/s12517-020-05906-6

Khan, M. Y. A., Gani, K. M., and Chakrapani, G. J. (2017). Spatial and Temporal Variations of Physicochemical and Heavy Metal Pollution in Ramganga River-A Tributary of River Ganges, India. *Environ. Earth Sci.* 76, 231. doi:10.1007/s12665-017-6547-3

Khan, M. Y. A., Khan, B., and Chakrapani, G. J. (2016). Assessment of Spatial Variations in Water Quality of Garra River at Shahjahanpur, Ganga Basin, India. *Arabian J. Geosciences* 9 (8), 1–10. doi:10.1007/s12517-016-2551-2

Kumar, A., Cabral Pinto, M., Candeias, C., and Dinis, P. A. (2021a). Baseline Maps of Potentially Toxic Elements on Soils of Garhwal Himalaya, India: Assessment of Their Eco-environmental and Human Health Risks. *Land Degradation & Development*. 32, 3856–3869. doi:10.1002/ldr.3984

Kumar, A., Kumar, M., Pandey, R., ZhiGuo, Y., and Cabral-Pinto, M. (2021b). Forest Soil Nutrient Stocks along Altitudinal Range of Uttarakhand Himalayas: An Aid to Nature Based Climate Solutions. *CATENA* 207, 105667. doi:10.1016/j.catena.2021.105667

Kumar, A., Taxak, A. K., Mishra, S., and Pandey, R. (2021c). Long Term Trend Analysis and Suitability of Water Quality of River Ganga at Himalayan hills of Uttarakhand, India. *Environ. Techn. Innovation* 22, 101405. doi:10.1016/j.eti.2021.101405

Larsen, F., Tran, L. V., Van Hoang, H., Tran, L. T., Christiansen, A. V., and Pham, N. Q. (2017). Groundwater Salinity Influenced by Holocene Seawater Trapped in Incised Valleys in the Red River delta plain. *Nat. Geosci* 10, 376–381. doi:10.1038/ngeo2938

Lee, J.-Y., and Song, S.-H. (2007). Evaluation of Groundwater Quality in Coastal Areas: Implications for Sustainable Agriculture. *Environ. Geol.* 52, 1231–1242. doi:10.1007/s00254-006-0560-2

Li, Y., Khan, M. Y. A., Jiang, Y., Tian, F., Liao, W., Fu, S., et al. (2019). CART and PSO+ KNN Algorithms to Estimate the Impact of Water Level Change on Water Quality in Poyang Lake, China. *Arabian J. Geosciences* 12 (9), 1–12. doi:10.1007/s12517-019-4350-z

Mishra, S., Kumar, A., and Shukla, P. (2021). Estimation of Heavy Metal Contamination in the Hindon River, India: an Environmetric Approach. *Appl. Water Sci.* 11 (1), 1–9. doi:10.1007/s13201-020-01331-y

Moss, S. A., Nagpal, N., and Branch, W. P. (2003). *Ambient Water Quality Guidelines for boron*. British Columbia, Canada: Water Protection BranchMinistry of Water, Land and Air Protection.

Ozsvath, D. L. (2009). Fluoride and Environmental Health: a Review. *Rev. Environ. Sci. Biotechnol.* 8 (1), 59–79. doi:10.1007/s11157-008-9136-9

Piper, A. M. (1953). *A Graphic Procedure in the Geochemical Interpretation of Water Analysis (No. 12)*. Ground Water Branch: US Department of the Interior, Geological Survey, Water Resources Division.

Pradhan, R. M., and Biswal, T. K. (2018). Fluoride in Groundwater: a Case Study in Precambrian Terranes of Ambaji Region, North Gujarat, India. *Proc. IAHS* 379, 351–356. doi:10.5194/piahs-379-351-2018

Pradhan, R. M., Guru, B., Pradhan, B., and Biswal, T. K. (2021). Integrated Multi-Criteria Analysis for Groundwater Potential Mapping in Precambrian Hard Rock Terranes (North Gujarat), India. *Hydrological Sci. J.* 66 (6), 961–978. doi:10.1080/02626667.2021.1906427

Ravenscroft, P., and McArthur, J. M. (2004). Mechanism of Regional Enrichment of Groundwater by boron: the Examples of Bangladesh and Michigan, USA. *Appl. Geochem.* 19 (9), 1413–1430. doi:10.1016/j.apgeochem.2003.10.014

Richards, L. A. (1954). *Diagnosis and Improvement of. Saline and Alkali Soils*. Handbook, 60.

Rosenthal, E. (1987). Chemical Composition of Rainfall and Groundwater in Recharge Areas of the Bet Shean-Harod Multiple Aquifer System, Israel. *J. Hydrol.* 89, 329–352. doi:10.1016/0022-1694(87)90185-5

Saleem, Q., and Algamal, Y. (2016). Assessment of Physico-Chemical and Biological Properties of Ground Water of Khulais, Province, Kingdom of Saudi Arabia. *Ijsrm. Human*. 5 (1), 504–521.

Schoeller, H. (1977). "Geochemistry of Groundwater," in *Groundwater Studies—An International Guide for Research and Practice*. Editors R. H. Brown, A. A. Konoplyantsev, J. Ineson, and V. S. Kovalensky (Paris: UNESCO), 1–18.

Singaraja, C., Chidambaram, S., Anandhan, P., Prasanna, M. V., Thivya, C., Thilagavathi, R., et al. (2013). Hydrochemistry of Groundwater in a Coastal

Region and its Repercussion on Quality, a Case Study-Thoothukudi District, Tamil Nadu, India. *Arab J. Geosci.* 7, 939–950. doi:10.1007/s12517-012-0794-0

Skrzypek, G., Dogramaci, S., and Grierson, P. F. (2013). Geochemical and Hydrological Processes Controlling Groundwater Salinity of a Large Inland Wetland of Northwest Australia. *Chem. Geology.* 357, 164–177. doi:10.1016/j.chemgeo.2013.08.035

Sonbul, A. R., Sharaf, M. A., Mesaed, A. A., and Ali, A. M. (20172017). Hydrogeology of Wadi Qudaid Area, Northeast Jeddah, West Central Arabian Shield, Saudi Arabia. *Ojg* 07, 1749–1766. doi:10.4236/ojg.2017.712117

Sun, H., Shi, B., Yang, F., and Wang, D. (2017). Effects of Sulfate on Heavy Metal Release from Iron Corrosion Scales in Drinking Water Distribution System. *Water Res.* 114, 69–77. doi:10.1016/j.watres.2017.02.021

Todd, D. K. (1959). *Groundwater Hydrology*. United States: John Wiley & Sons, 535.

USEPA (2008). Regulatory Determinations Support Document for Selected Contaminants from the Second Drinking Water. Contaminant Candidate List (CCL2); EPA 815-R-08-012. Washington, DC: Office of Water.

USEPA (2014). Announcement of Preliminary Regulatory Determinations for Contaminantson the Third Drinking Water Contaminant Candidate List; Proposed Rule. *Fed. Regist.* 79 (202), 62715–62750.

Vengosh, A., and Rosenthal, E. (1994). Saline Groundwater in Israel: its Bearing on the Water Crisis in the Country. *J. Hydrol.* 156, 389–430. doi:10.1016/0022-1694(94)90087-6

Wada, Y., van Beek, L. P., van Kempen, C. M., Reckman, J. W., Vasak, S., and Bierkens, M. F. (2010). Global Depletion of Groundwater Resources. *Geophy Res. Lett.* 37, 1–5. doi:10.1029/2010gl044571

Wang, W.-L., Wu, Q.-Y., Wang, C., He, T., and Hu, H.-Y. (2015). Health Risk Assessment of Phthalate Esters (PAEs) in Drinking Water Sources of China. *Environ. Sci. Pollut. Res.* 22, 3620–3630. doi:10.1007/s11356-014-3615-z

Weast, R. C. (1985). *CRC Handbook on Chemistry and Physics*. Boca Raton: CRC Press.

Who (1994). *Guidelines for Drinking Water Quality*, 1. Geneva: World Health Organisation.

Who (2004). *Guidelines for Drinking-Water Quality*. 3rd edn., Vol. 1. Geneva: World Health Organisation, 515.

Who (2011). *Guidelines for Drinking-Water Quality*. Geneva: World HealthOrganization.

Who (2017). *Guidelines for drinking-water quality: fourth edition incorporating first addendum, 4th ed + 1st add*. World Health Organization. Available at: https://apps.who.int/iris/handle/10665/254637.

Who (1993). *World Health Organization), Guidelines for Drinking Water Quality; Volume1. 1,Recommendations*. 2nd. Geneva.

World Weather Online (2021). Available at: https://www.worldweatheronline.com/.

Wu, J., and Sun, Z. (2016). Evaluation of Shallow Groundwater Contamination and Associated Human Health Risk in an Alluvial plain Impacted by Agricultural and Industrial Activities, Mid-west China. *Expo. Health* 8 (3), 311–329. doi:10.1007/s12403-015-0170-x

Yin, Z., Duan, R., Li, P., and Li, W. (2021). Water Quality Characteristics and Health Risk Assessment of Main Water Supply Reservoirs in Taizhou City, East China. *Hum. Ecol. Risk Assess. Int. J.* 27 (8), 2142–2160. doi:10.1080/10807039.2021.1958670

Zarhloule, Y., Fekkoul, F., Boughriba, M., Kabbabi, A., Carneiro, J., Correia, A., et al. (2009). Climate Change and Human Activities Impact on the Groundwater of the Eastern Morocco: Case of Triffa Plain and Shallow coastalM Editerranean Aquifer at Saïdia. Innovation in Groundwater Governance in MENA Region. *JSIW* 13, 14–17.

Conflict of Interest: The authors declare that the research was conducted in the absence of any commercial or financial relationships that could be construed as a potential conflict of interest.

Publisher's Note: All claims expressed in this article are solely those of the authors and do not necessarily represent those of their affiliated organizations, or those of the publisher, the editors and the reviewers. Any product that may be evaluated in this article, or claim that may be made by its manufacturer, is not guaranteed or endorsed by the publisher.